IMPROVING NEURAL RECORDING TECHNOLOGY AT THE NANOSCALE

A DISSERTATION
SUBMITTED TO THE FACULTY OF THE GRADUATE SCHOOL
OF THE UNIVERSITY OF MINNESOTA
BY

JOHN ERIC FERGUSON

IN PARTIAL FULFILLMENT OF THE REQUIREMENTS
FOR THE DEGREE OF
DOCTOR OF PHILOSOPHY

ADVISOR: A. DAVID REDISH

AUGUST, 2011

Acknowledgments

Thanks to all the members of the Redish lab for their advice, help, and friendship: Chris Boldt, Matthijs van der Meer, Zeb Kurth-Nelson, Jadin Jackson, Adam Steiner, Kelsey Seeland, Andy Papale, Nate Powell, Andrew Wikenheiser, Jeff Stott, Anoopum Gupta, Adam Johnson, Beth Masimore, and Neil Schmitzer-Torbert. Special thanks to A. David Redish, my advisor, for his enthusiastic mentorship and guidance through the whole doctoral research experience, for encouraging me to pursue some pretty crazy research ideas, and for leading by example.

Thanks to the members of my thesis committee: Matthew Johnson, Theoden Netoff, A. David Redish, and LiLian Yuan. Also, thanks to my fellowship co-advisors, Art Erdman and Bin He, and to the other members of my fellowship committees: Geoff Ghose, Teresa Nick, Theoden Netoff, Will Durfee, and David Odde.

I would also like to acknowledge my research collaborators for expanding the boundaries of our research: Art Erdman, Khaled Al-Ashmouny, Euisik Yoon, Kevin Crisp, Joshua Puhl, Karen Mesce, Tyler Stigen, and Theoden Netoff.

During my graduate studies at the University of Minnesota, I received sup-

port from the Institute for Engineering in Medicine, the NIH Neuro-Physical-Computational Sciences Training Grant (T90 DK70106), the NIH Neuroimaging Training Program (T32 EB008389), and the University of Minnesota Interdisciplinary Doctoral Fellowship. Parts of this work were carried out in the University of Minnesota Nanofabrication Center and Characterization Facility, which receive partial support from NSF through the NNIN program.

Special thanks to the numerous friends and family who supported me and kept me excited about living and performing research in Minnesota, especially to my parents, Tom and Amalia Ferguson.

Abstract

Neural recording electrodes are widely used to study normal brain function (e.g., learning, memory, and sensation) and abnormal brain function (e.g., epilepsy, addiction, and depression) and to interface with the nervous system for neuroprosthetics. With a deep understanding of the electrode interface at the nanoscale and the use of novel nanofabrication processes, neural recording electrodes can be designed that surpass previous limits and enable new applications. In this thesis, I will discuss three projects. In the first project, we created an ultralow-impedance electrode coating by controlling the nanoscale texture of electrode surfaces. In the second project, we developed a novel nanowire electrode for long-term intracellular recordings. In the third project, we created a means of wirelessly communicating with ultra-miniature, implantable neural recording devices. The techniques developed for these projects offer significant improvements in the quality of neural recordings. They can also open the door to new types of experiments and medical devices, which can lead to a better understanding of the brain and can enable novel and improved tools for clinical applications.

Contents

List of Figures

Chapter 1

Introduction

> *Esse quasi nanos gigantium humeris insidentes, ut possimus plura eis et remotiora videre, non utique proprii visus acumine aut eminentia corporis, sed quia in altum subvehimur et extollimur magnitudine gigantea.*
>
> We are like dwarfs on the shoulders of giants, so that we can see more than they and things at a greater distance, not by virtue of any sharpness of sight on our part or any physical distinction, but because we are carried high and raised up by their giant size.
>
> Bernard of Chartres (documented by John of Salisbury in 1159)

The phrase "standing on the shoulders of giants" is often attributed to Isaac Newton as a respectful statement about his dependence on the work of his predecessors (or perhaps, as recently suggested, a veiled insult referring to a competing scientist's small size and hunched back). However, the phrase is much older than that. It was first documented by John of Salisbury in 1159 in reference to the great debate at the time as to whether the 'modernists' (as they called themselves then,

and how we think of ourselves now too) would be able to create works that were as great as the 'ancients', scholars from Ancient Greece and Rome (Stock, 1979).

Over the past millennium, "standing on the shoulders of giants" has became a popular saying and an elegant way of illustrating how collaboration and interdependency allow for the best perspective, rather than any single person's ability. Thus, it is a fitting motto for modern scientific research, where we are all dependent on the genius and hard work of our scientific predecessors and colleagues.

I have also chosen to include the quote in its original form because it shows the latin forms of the words 'giant' and 'dwarf', *giga* and *nano* (both underlined above). These terms are commonly used as prefixes to describe a billion or a billionth, respectively. In this thesis, both prefixes will be used frequently. Even though *giga* and *nano* are on opposite extremes of scale, these terms are together critical in understanding and using modern neural recording devices. In this thesis, we will often talk about gigaohms (GΩ) and nanometers (nm) in the same sentence.

This thesis emphasizes the importance of thinking about neural recording devices on the nanoscale. This is the scale that the neuron works on, the size of many of its internal components, such as the cell membrane, which is a few nanometers thick. Proteins and neurotransmitters are also on the nanoscale. Up until recently, most neural devices were constructed on the microscale because this was the scale that could be seen using visible light under a microscope. With the development of nanofabrication methods and nanoscale imaging techniques, we now have the opportunity to rethink the old methods of recording from neurons.

At the same time, by working at the nanoscale, we are creating effects on the gigascale. Specifically, the resistance of the electrode can reach many gigaohms when the size of the electrode is in the nanoscale. Such a large resistance can create many challenges (and some advantages) in neural recordings. Methods of minimizing the resistance of nanoscale recording electrodes (or at least minimizing the negative effects of the huge resistance) is a critical challenge with nanoelectrodes and is an important part of this thesis.

The combined task of minimizing the size and resistance of electrodes is important in creating a new generation of recording electrodes that has the potential to create new applications and to open up novel avenues of scientific research. As stated by Purves (1981), "The history of microelectrode technology can be regarded as a succession of attempts to minimize tip diameter and resistance simultaneously". This thesis attempts to stand on the shoulders of giants and to look at the nanoscale.

This thesis begins by describing both conventional intracellular and extracellular techniques (Chapters 2 and 3). Both techniques have been extremely successful in providing us with great insights in neuroscience and numerous discoveries on the electrical behavior and function of neurons. These chapters will focus on creating an understanding at an electrical level of how intracellular and extracellular neural recordings work. Additionally, they will include discussion about the current limitations of both methods. Chapters 4, 5, and 6 will describe our novel contributions to neural recording technology. They will follow and expand upon our journal articles that have been published (Chapters 4 and 6) or are under re-

view at the time of writing this thesis (Chapter 5). Chapter 4 describes a new nanoscale coating that we developed to improve extracellular recordings. Chapter 5 describes a novel type of intracellular recording device, based on nanowire electrodes. Chapter 6 describes a new wireless communication system that allows for communication with ultra-miniature, implantable neural recording devices that can potentially be the same size as neurons. The thesis will conclude with Chapter 7, where I will speculate on some potential future directions of neural recording technology.

Chapter 2

Conventional intracellular recording

Intracellular neural recordings measure the voltage across and/or the currents through a neuron's cell membrane. This type of recording is the foundation for a range of neuroscientific and pharmacological studies and is widely used to investigate the behavior of neurons at a detailed level. There are numerous guides and books that comprehensively describe acquisition hardware, techniques, and other topics in intracellular recording (Geddes, 1972; Ferris, 1974; Purves, 1981; Brown and Flaming, 1986; Sherman-Gold, 1993). This chapter will describe the main types of intracellular recording techniques, provide a detailed equivalent circuit of the cell-electrode interface, and comment on factors that may affect the faithfulness of recording. This chapter will focus on presenting the electrode-neuron interface in a context that will help frame our experiments that will be described in Chapter 5.

2.1 Types of intracellular electrodes

Intracellular recording electrodes can be categorized into two types: sharp and patch. Sharp microelectrodes penetrate the neuron and patch microelectrodes seal on to the neuron's cell membrane to create a recording interface. Each type of electrode has its own advantages, disadvantages, and history. Both types are still widely in use today.

2.1.1 Sharp microelectrodes

The vast majority of sharp microelectrodes used for intracellular recordings are made from electrolyte-filled glass micropipettes. These micropipettes were first used for recording from cells by Ettisch and Péterfi (1925) who drew glass tubing into micropipettes with tip diameters of $10\,\mu m$ and filled them with $0.1\,mol\,L^{-1}$ potassium chloride in agar. Soon after, glass micropipettes were drawn to almost $1\,\mu m$ by Gelfan (1926). Over the next few decades, various methods of pulling (automatically and manually) the glass micropipettes and filling solutions were developed. The electrical properties and recording quality of these glass microelectrodes are highly dependent on the tip geometry, glass type, filling solution, and many other parameters. The specific cell type, preparation, and preferences of the scientist often dictated the specific parameters used.

The primary function of sharp microelectrodes is to penetrate a neuron without causing damage, but they often cannot penetrate a cell's membrane by themselves. When a sharp micropipette is pushed into a neuron, the cell's membrane might

dimple under the applied force and not allow the micropipette into the cell's interior. Scientists have a few options in order to encourage penetration into the cell. They can apply mechanical vibration in the form of tapping the micromanipulator (or, perhaps in frustration, by jumping up and down on the floor), which sometimes works but is unreliable and difficult to control. Another option is to apply a high-frequency oscillating current (called "buzzing") or by applying positive or negative step currents.

In a sharp intracellular recording, the amplifier measures the difference in potentials of the electrode in a micropipette that is electrically connected to the cytoplasm within the cell membrane to a reference electrode far away from the cell but in the same conductive, environmental fluid. There is a resistance to current flowing from the cytoplasm of the cell to the electrode in the stem of the glass micropipette. This resistance is dependent on the diameter of the tip and the geometry of the micropipette. A smaller-diameter microelectrode has a larger tip resistance. There is also a capacitance between the inside and outside of the micropipette. This capacitance is distributed across the tip resistance. As will be described later, this capacitance can be a significant source of recording errors.

A comprehensive circuit diagram can be seen in Figure 2.1. As can be seen, most of the circuit is represented by resistors, capacitors, and batteries. Although the circuit can be simplified as will be discussed later, it is important to describe all variables that are involved in all the components of intracellular recording in order to understand how the entire system works and to understand the source of errors in both conventional recording methods (discussed in this chapter) and

novel recording methods (discussed in later chapters).

The electrode in the micropipette is represented by C_{ma}, R_{ma}, R'_{ma}, C'_{ma}, and E_{ma}. The interface between the electrode and the electrolyte in the pipette is complex and has both resistive and capacitive components. This circuit shows two resistors and two capacitors, both in series and in parallel, to better represent the complicated frequency dependency of the overall impedance of the electrode. In reality, this is only an approximation, and the complex impedance is best determined experimentally using electrical impedance spectroscopy with a potentiostat. E_{ma} is the electrode's half-cell potential, which is an inherent property of all electrodes and is dependent on the nearby ionic concentration, type of metal, and temperature of the interface. In practice, most intracellular recording electrodes use chlorided silver/silver-chloride (Ag/AgCl) wires. This type of electrode is close to a perfectly non-polarizable electrode, meaning it allows for current to be freely conducted across the electrode-electrolyte interface. In addition to being low impedance, Ag/AgCl electrodes have stable half-cell potentials (E_{ma}), and the chloride ion that is formed in redox reactions is common in neurons. If there is insufficient chloriding of the silver wire or a bad connection, the impedance of the electrode increases significantly and the half-cell potential becomes unstable, creating many problems in recordings.

The reference electrode is represented by C_{mb}, R_{mb}, R'_{mb}, C'_{mb}, and E_{mb}. This electrode is very similar to the electrode in the micropipette and is also usually made of Ag/AgCl. Similar problems due to insufficient chloriding or bad connections can also occur with the reference electrode. However, the half-cell potential

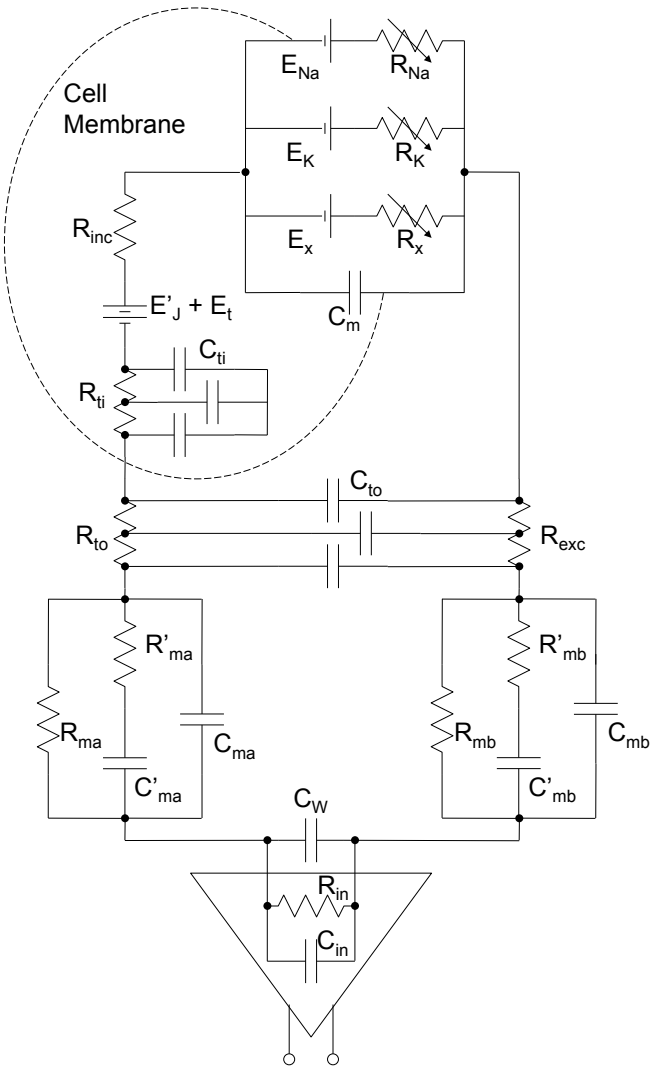

Figure 2.1: *A complete circuit diagram of a sharp intracellular recording. Figure based on Geddes (1972).*

of the reference electrode may not equal the micropipette electrode, causing some errors in recording. In order to equilibrate the two half-cell potentials (for an experimenter who is very concerned with exact values of potential recordings), the micropipette and reference electrodes can be connected in a solution before the experiment.

The wires connecting the micropipette electrode and the reference electrode to the amplifier may have a capacitance between them. This is represented by C_W. If C_W is large, it may cause errors in recording. In order to minimize C_W, the length of wire from the electrodes to the amplifier (or amplifier headstage) should be minimized.

The amplifier is represented by R_{in}, the input resistance, and C_{in}, the input capacitance. These elements should be large to minimize distortion of the measured signal. Most modern amplifiers are designed to have impedances much larger than the impedances of the electrodes to eliminate this problem. However, if the electrodes for a specific application and impedances that are too large for the amplifier, the input resistance and input capacitance of the amplifier can be problematic.

The portion of the micropipette tip that is outside of the cell is represented by R_{to}, C_{to}, and R_{exc}. R_{to} is the resistance of the solution in the micropipette tip that is outside of the cell. Distributed across this length, C_{to} is the capacitance of the inside of the micropipette to the outside solution, which is shown as the distributed resistance R_{exc}. This capacitance can cause significant errors in a recording and cannot be ignored.

The cell membrane is represented by C_m, E_k, R_k, E_{Na}, R_{Na}, E_x, and R_x.

These elements refer to the elements of a Hodgkin-Huxley model neuron (Hodgkin and Huxley, 1952).

Inside the cell, the relevant circuit elements are R_{ti}, C_{ti}, R_{inc}, E'_J, and E_t. Similar to the portion of the micropipette outside the cell, the resistance of the tip, R_{ti} is distributed and capacitively connected by C_{ti} to the resistance of the solution inside the cell, R_{inc}. R_{ti} is important, because the tip resistance can be very large for small diameter micropipette tips. C_{ti}, on the other hand, is not important because the potential difference across the micropipette tip within the membrane should be zero. E'_J is the liquid-junction potential and arises when there is a difference in the ions or concentration of ions in the micropipette and in the cytoplasm of the cell. It is not dependent on the diameter of the tip. E_t is the tip potential and also depends on the difference in ions or concentration of ions. In addition, it also depends on the tip diameter, glass type and thickness, and micropipette geometry.

The circuitry of a traditional sharp intracellular recording can be simplified, as shown in Figure 2.2. For a sharp intracellular recording, the most important circuit elements are the tip resistance (R_t), distributed tip capacitance (C_d), electrode potentials (E_{ma} and E_{mb}), tip potential (E_t), and liquid-junction potential (E'_J). If everything is set-up properly and traditional components are used, the other circuit elements can be ignored. Figure 2.2A shows a simplified circuit where the capacitance is distributed across the tip resistance. This distributed circuit is closer to the full circuit. Figure 2.2B shows a circuit simplification with lumped parameters rather than distributed elements, which is easier to use for circuit analyses.

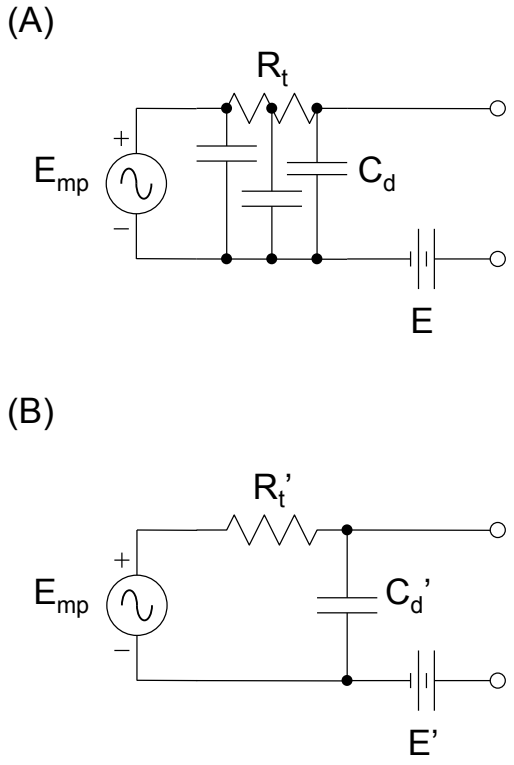

Figure 2.2: *Simplified circuit diagrams of a sharp intracellular recording. (A) shows a the circuit with distributed parameters. (B) shows the circuit with lumped parameters. Based on Geddes (1972).*

2.1.2 Patch microelectrodes

Patch microelectrodes are a newer form of intracellular recording electrode. They were developed by Neher and Sakmann (1976), who won the Nobel Prize in Physiology or Medicine in 1991 for this work. This technique used glass micropipettes with larger diameters than traditional sharp microelectrodes. The micropipettes were pressed up against the neuron's cell membrane, forming a seal around a patch of membrane. The seal had a resistance of megaohms. The cell was then 'voltage-clamped', meaning it was maintained at a specific voltage, allowing for the measurement of currents through single ion channels in the membrane. Several important improvements to patch microelectrodes were achieved by Neher and Sakmann and their colleagues after the original paper was published. One of the most important improvements was the creation of a 'giga-seal' by applying suction to the membrane patch. This giga-seal increased the resistance of the seal from megaohms to gigaohms, resulting in a significant improvement in the quality of isolation and recording. The reasons for this improvement will be discussed in greater detail later when the equivalent circuit is introduced. In addition, the giga-seal allows for 'current-clamp' recording, where the current is maintained at a specific value and the voltage is measured. This type of recording is similar to the type of current produced by a synaptic input.

Patch clamping allows for many recording configurations, which were first elaborated by Hamill et al. (1981). Figure 2.3 shows the main types of patch-clamp recording configurations and the sequence of obtaining these configura-

tions.

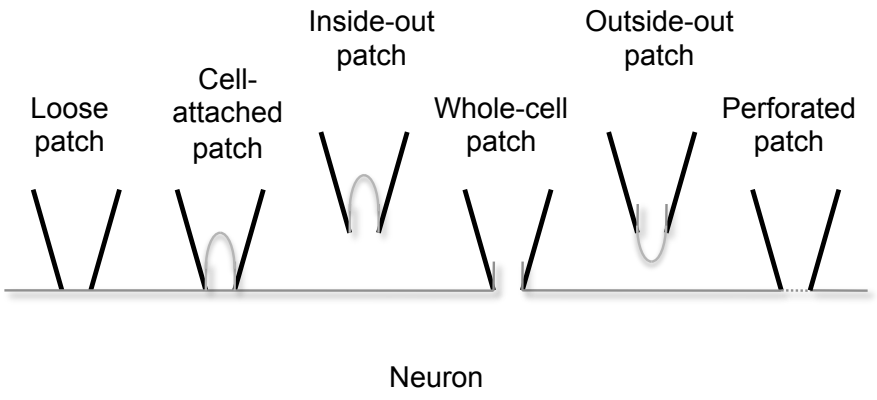

Figure 2.3: *The main configurations of intracellular recordings obtained with a patch microelectrode. When a micropipette first patches a cell, it is in cell-attached patch configuration. A loose-patch refers to a cell-attached patch with little or no applied suction. The micropipette can then be removed from the cell producing an inside-out patch configuration. Otherwise, the membrane can be ruptured from the cell-attached patch configuration to produce a whole-cell configuration. From there, the micropipette can be moved away from the cell to make an outside-out patch. The final configuration, the perforated patch configuration, uses antibiotics in the micropipette filling solution to produce pores in the membrane. Figure based on Hamill et al. (1981) and Ypey and DeFelice (2011).*

When the patch pipette is pressed up against a cell, the configuration is called cell-attached patch. With suction applied, a gigaohm seal can be formed. This allows for high quality recording of currents within the sealed membrane patch. When little or no suction is applied, this configuration results in a 'loose-patch'

recording. Although a loose-patch configuration does not have the advantage of improved recording quality of configurations with giga-seals, it does have a few advantages. The cell-attached patch configuration is relatively easy to obtain and can be performed on cells that are difficult to obtain a gigaohm seal. Cell-attached patch also can be performed multiple times on a single cell. Because it does not cause significant damage to the membrane, the micropipette can be repositioned several times.

If the micropipette is pulled away from the cell in the cell-attached patch configuration, an inside-out patch is formed. This configuration allows for studies of the membrane patch away from the cell. The cell may reseal after the patch is removed, allowing for other recordings from the same cell at a later time. This configuration is called the IOP because the side of the membrane patch that was formerly inside the cell is now in contact with the solution outside of the cell.

If strong suction is applied to a cell-attached patch configuration, the cell membrane ruptures, creating a whole-cell configuration. This configuration allows for a direct connection between the solution inside the micropipette with the inside of the cell. It is called a whole-cell configuration because it allows for access inside the entire cell, rather than just a patch membrane. The whole-cell configuration allows for high quality recordings of neuronal activity over the whole cell rather than just a membrane patch, but it damages the neuron because the membrane must be ruptured. The ruptured membrane causes the solution in the micropipette to enter into the cell and the contents of the cell to enter the micropipette. This leaking is called ‘dialysis’ of the cell and usually results in cell death within a

brief period of time, usually in minutes to an hour.

If the micropipette is slowly pulled away from the cell after a whole-cell configuration, an outside-out patch is formed. This is similar to the inside-out patch configuration in that it also allows for studies of the membrane patch away from the cell. However, the outside-out patch flips the orientation of the membrane patch, so the side that was originally outside the cell remains in contact with the solution outside the cell. This technique causes more damage to the cell than an inside-out patch and multiple recordings cannot typically be performed on the same cell.

The final configuration, developed by Horn and Marty (1988), is the permealized patch whole cell or perforated patch configuration. In this configuration, an antibiotic is introduced into the micropipette filling solution. The antibiotic causes pores to form in the membrane patch, allowing for a direct electrical connection between the micropipette and the cell's interior, without dialyzing the cell. However, the perforated membrane has greater access resistance than a whole-cell configuration, resulting in a lower quality recording.

Figure 2.4 shows the equivalent circuits that correlate to the various recording configurations.

The patch-clamp amplifier is represented by a voltage source (E_{pc}) with a series resistance (R_{pc}), and a parallel capacitance (C_{pc}). Just as in the case with the sharp intracellular recording amplifier, the input impedance of the patch-clamp amplifier must be much larger than the impedance of the microelectrode to avoid distortion.

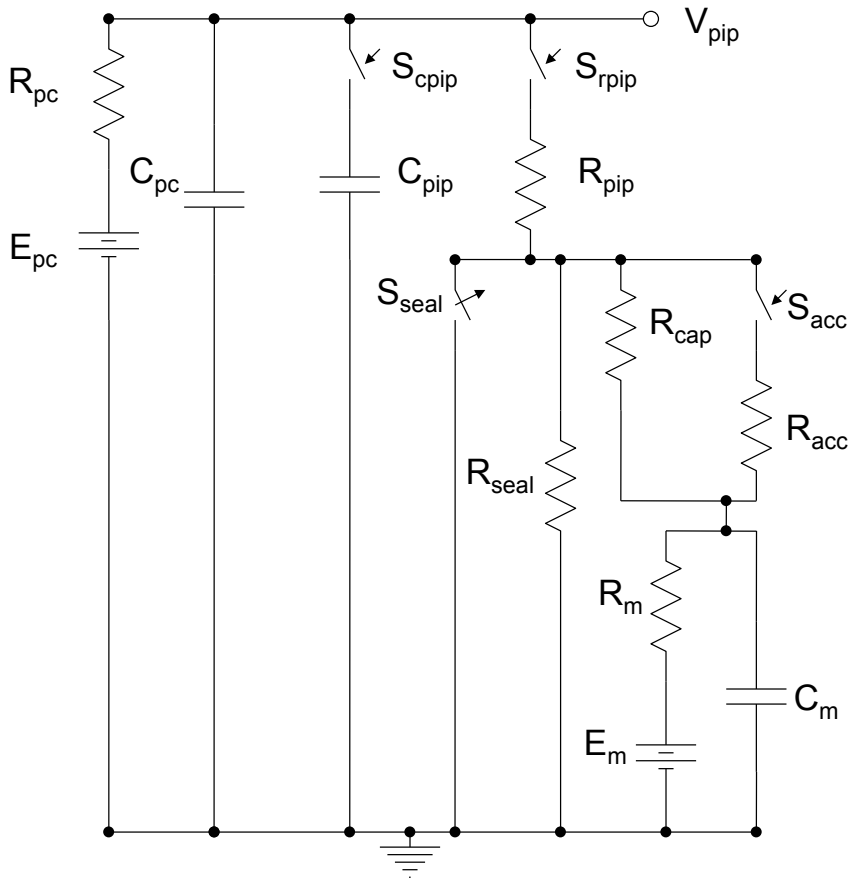

Figure 2.4: *The equivalent circuits of the recording configurations of patch microelectrodes based on Ypey and DeFelice (2011). When the micropipette enters the bath, switches S_{cpip} and S_{rpip} close. When suction is applied and a cell-attached configuration is achieved, switch S_{seal} opens. If the membrane is ruptured, producing a whole-cell configuration, switch S_{acc} closes.*

When the patch micropipette enters the bath, it is represented by a resistor (R_{pip}) in parallel with a capacitor (C_{pip}). Switches S_{cpip} and S_{rpip} are closed in Figure 2.4.

Next, when the micropipette touches the cell and suction is applied, a cell-attached patch configuration is obtained. This is represented by switch S_{seal} opening, which eliminates the direct connection of the micropipette to the grounded solution. In its place, the micropipette is connected to the cell by a resistor (R_{cap}) with the seal resistance in parallel (R_{seal}). A giga-seal refers to the case when R_{cap} has a value of GΩs.

The cell is represented by a voltage source (E_m), a series resistor (R_m), and a parallel capacitor (C_m). For a more detailed circuit, the cell can be represented by a Hodgkin-Huxley model parameters C_m, E_k, R_k, E_{Na}, R_{Na}, E_x, and R_x as in Figure 2.1.

When the membrane is ruptured, a whole-cell configuration is formed. This is represented by closing switch S_{acc}. This causes the access resistance (R_{acc}) to lower the resistance between the micropipette and the cell.

2.2 Intracellular recording difficulties

Even though sharp and patch intracellular recordings are powerful and widely used, they are often performed without an understanding of their limitations.

2.2.1 Electrical errors

Intracellular recordings can have electrical errors that cause a inaccurate measurement of the cell's electrical activity. The membrane potential or currents recorded could be significantly different than the real values. The electrical properties of the electrode, cell, and amplifier could cause a distortion in the signal recorded. For example, with an uncorrected liquid-junction potential, the measured resting membrane potential could be different than the real resting membrane potential. Other electrical errors could also cause unwanted filtering of the signal or an attenuation in the magnitude of action potentials or synaptic potentials. With the use of the equivalent circuits that were described in the previous section, the sources and remedies for these electrical errors can be understood.

Most sources or recording error can be partially or completely compensated or eliminated using modern amplifiers. Large values of tip resistance or capacitance can cause waveform distortion or signal attenuation. These circuit elements are shown as R_t and C_d in Figure 2.2 and as $R_{pip} + R_{cap}$ or $R_{pip} + R_{acc}$ (depending on the recording configuration) and C_{pip} in Figure 2.4. The tip resistance and capacitance act as elements in a voltage divider circuit and can significantly reduce and modify the signal measured by the amplifier. In modern amplifiers, there are built in feedback circuits that compensate for non-negligible values of tip resistance and capacitance. However, these compensation circuits do not work perfectly; they are best suited to compensating for small or slow changes (Sherman-Gold, 1993).

It is also important for experimenters to realize how dependent the quality of the recording is on their methods of setting up the intracellular recording. There are numerous small details for the experimenter to ensure. Most of these can be learned from (Sherman-Gold, 1993) and from experience. However, I will mention two important ones here. Errors due to the liquid-junction potential can create misleading measurements of the membrane resting potential. In order to minimize this effect, great care should be made to choose the micropipette filling solution to closely match the types and concentrations of ions inside the cell (for a whole-cell patch or sharp intracellular recording) or the ions outside the cell (for a cell-attached recording). Also, in order to minimize stray and shunting capacitances, which low-pass filter the recorded signal, wires should be kept short and micropipette immersion depth should be minimized. If capacitance continues to be a problem, thicker glass or an insulating coating can be used in the micropipette.

One type of error that cannot be compensated using sophisticated modern amplifiers or proper methods is the problem of space clamping. Improper space clamping occurs when one part of the cell is clamped to a specific voltage and more distant parts of cells, such as dendrites or axons, are at different voltages. This difference in potentials is caused by the axial resistance of the cell membrane. Cells that are not completely voltage clamped may act differently than expected. Currents injected into the soma in a whole cell patch clamp configuration may be significantly different than the currents that affect the distant parts of cells. This can create significant errors in synaptic and other important currents.

There is currently no good way of minimizing the problem. The best alternatives are to choose cells that are less prone to space-clamp problems or to cut or tie off sections of cells that are problematic when space-clamping might cause significant errors.

For most applications, these sources of error are not a significant problem. However, it is important to know that they exist and to identify the occasions that could affect the results.

2.2.2 Cell damage

Intracellular recordings can greatly affect or damage cells that are being recorded. Because it is important for a measurement not to affect the underlying process that is being measured, the types and extent of cell damage should be understood by experimenters. In addition, methods of minimizing cell damage should be used when possible.

Both sharp and patch microelectrodes can damage cells. In general, sharp micropipettes and cell-attached patch configurations cause less damage than whole-cell recordings because of the dialysis of the cell discussed above. However, all types of intracellular recordings disturb both the cell membrane and its embedded proteins by puncturing, pressing, or rupturing a part of the membrane. In addition, organelles inside the cell can also be damaged. To minimize the damage of cells using patch micropipettes, looser seals can be used, but this can cause problems with the quality of electrical recordings. For sharp micropipettes, smaller diame-

ter sharp electrodes can be used. The use of nanowires for this purpose is the topic of Chapter 5.

Chapter 3

Conventional extracellular recording

Extracellular neural recordings measure the electrical field potentials that are generated outside of neurons. Extracellular recordings detect action potentials and local field potentials from nearby neurons and have enabled an enormous number of discoveries about the functional dynamics of neurons in motor, sensory, and cognitive studies.

Extracellular recordings have several unique advantages over intracellular recordings. The biggest is that extracellular electrodes can record from preparations that are difficult or impossible using intracellular microelectrodes, such as in freely moving animals. Extracellular recordings are generally easier to perform than intracellular recordings and require less sophisticated equipment and techniques. They can also record from several cells simultaneously, allowing for simultane-

ous recordings of large neural ensembles. Extracellular recording electrodes also cause much less damage to cells than intracellular electrodes and thus can record signals for much longer, up to months or years, instead of minutes to hours.

On the other hand, extracellular recordings have some disadvantages compared to intracellular recordings. They are more difficult to interpret than intracellular recordings because they are an indirect measurement of neuronal membrane currents or voltages, while intracellular microelectrodes directly measure these signals. Intracellular recordings can measure subthreshold events and resting membrane potentials, as well as action potentials, while extracellular recordings are primarily used for detecting action potentials and local field potentials. In addition, intracellular techniques allow for current and voltage clamping of neurons and permit labeling of neurons for future reconstruction of their morphologies and connectivities.

This chapter will describe the relationship between transmembrane potentials and extracellular potentials, then describe the main types of extracellular recording electrodes including an equivalent circuit, and finally describe the limitations of current extracellular recording technology.

3.1 Origin of extracellular fields

The complex relationship between intracellular and extracellular potentials has been studied since at least 1957 (Fatt, 1957). Soon after that study, there was wide disagreement as to the nature of this relationship (Freygang and Frank,

1959), specifically which parts of the cell were responsible for the action potentials seen extracellularly and whether the extracellular signal was equivalent to the intracellular signal or its first or second derivative. Simultaneous intracellular/extracellular studies that were performed on various locations in cell membrane revealed the complexity of the relationship; certain phases of the extracellular action potential were due to activity from different parts of the cell and passive spreading of signal across the membrane (Terzuolo and Araki, 1961). Even recent, well-controlled studies of simultaneous intracellular and extracellular recordings in anesthetized animals (Henze et al., 2000) have not helped to simplify our understanding of the relationship.

In addition, recent modeling studies have further revealed the complexity of the intracellular/extracellular relationship. The most comprehensive modeling study to date used a compartmental model of a neuron to calculate the extracellular potential field generated by each component (Gold et al., 2006, 2007). The components were calculated with Hodgkin-Huxley style models with twelve to fifteen different voltage-dependent ionic currents and programmed to match the signals from a simultaneous intracellular/extracellular recording experiment in anesthetized rats (Henze et al., 2000). However, it was found that matching signals from extracellular recordings was much more difficult than matching signals from intracellular experiments. The intracellular signal was primarily dependent on the local environment of the compartment from which it was recording whereas the extracellular signal was affected by the distribution of ion channels and the activation of distant regions of the cell. Even the morphology of neurons was shown

to affect the amplitude of extracellular signals. Thus, even complex computational models have difficulty fully explaining extracellular neural fields.

Another computational approach evaluated the accuracy of approximations for extracellular signals. Milstein and Koch (2008) performed a multipole expansion of the signals generated by the multi-compartment model from Gold et al. (2006, 2007) and found that the first 25 moments were necessary to approximate the extracellular signal within $500\,\mu$m from center of the neuron, while a much simpler dipole approximation was valid when further than $1\,$cm from the center of the cell. Another approach, comparing extracellular recordings to scanning electron microscopy images of brain slices, found signals from dipole approximations matched 95% of the power from the extracellular recordings (Mechler and Victor, 2011; Mechler et al., 2011). It was concluded that at typical distances between extracellular electrodes and cells, the dipole was a good approximation to determine the location of cells. However, this study focused on identifying the distance to cell from an extracellular electrode and not on explaining the waveform of the extracellular signal.

To briefly summarize, the origin of extracellular fields is complex. There are some similarities between the signals from intracellular and extracellular recordings, but these similarities are limited and depend greatly on experimental conditions and the characteristics of the individual cell. However, with some assumptions, approximations can be made for specific purposes, such as to determine the distance from an electrode to the center of a cell. Overall, extracellular recordings are significantly different than intracellular recordings and should be treated

differently. Extracellular signals certainly relate to the activity, morphology, and features of a cell, but this relationship is difficult to ascertain. Therefore, conclusions about the internal dynamics of neurons determined by extracellular signals must be made very carefully.

3.2 Extracellular electrodes for recording from freely moving animals

Neural recording technology used in freely moving animals has proven to be a powerful tool for neuroscience research. The first extracellular recording in a freely moving animal was performed over fifty years ago by Strumwasser (1958). He was studying ground squirrels as they hibernated. He used $80\,\mu$m-diameter stainless-steel wires that were insulated except for the tip to perform recordings that were stable for several weeks. During this time, the squirrels slept, ran around, and even adjusted their bedding. Several years later, O'Keefe and Dostrovsky (1971) used a similar system with glass-insulated platinum-plated tungsten wire electrodes to discover place field activity in hippocampal neurons in rats.

More recently, the development of multielectrode recording technology has allowed for improved discrimination among many simultaneously recorded neurons. Two types of microwire-based multielectrodes, the stereotrode and the tetrode, have been successfully used for recording from neural ensembles in freely moving animals for many decades. Stereotrodes are bundles of two microwires

(McNaughton et al., 1983), and tetrodes are bundles of four microwires (Wilson and McNaughton, 1993; O'Keefe and Recce, 1993; Gray et al., 1995) that allow for separation of signals from multiple nearby neural sources. Multiple independently movable stereotrodes or tetrodes can be implanted in the brain of freely moving animals and can enable recordings of local field potentials or action potentials from hundreds of individually discriminable neurons simultaneously.

Another class of microelectrode recording devices uses microfabrication technology. This project began in the late 1960's and has recently resulted in commercially available microelectrodes (Wise et al., 1970; Wise, 2007). Microfabricated multielectrode array technology has the advantages of reproducibility and fixed geometry (including fixed electrode diameters and spacing). However, microfabricated electrodes have been problematic for long-term chronic recordings in freely moving animals. Thus, most labs continue to use microwire microelectrodes (stereotrodes and tetrodes) for long-term, chronic recordings.

3.3 Equivalent circuits

Figure 3.1 shows an equivalent circuit of an extracellular recording electrode based on Nelson et al. (2008), which was based on Robinson (1968). The electrode detects the extracellular signal (V_{sig}) as it passes through the electrode impedance (Z'_e) and the amplifier impedance (Z'_a) to ground.

The electrode's overall impedance (Z'_e) is comprised of several components. R_S is the resistance of the extracellular solution. R_m is the resistance of the metal

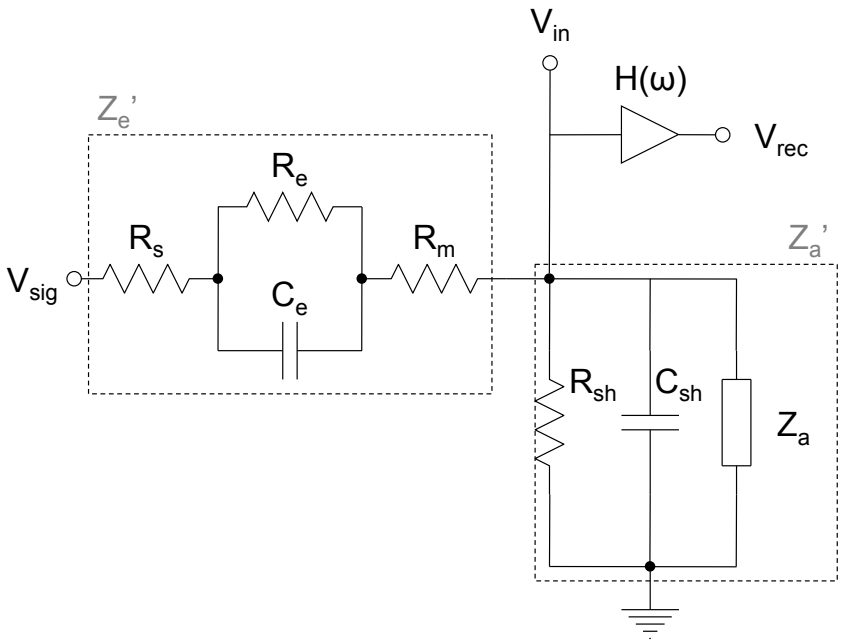

Figure 3.1: *Equivalent circuit for an extracellular recording. Based on Nelson et al. (2008) and Robinson (1968).*

of electrode, which is usually very small relative to the other impedances in the electrode. The electrode-electrolyte interface is represented by the parallel resistor and capacitor R_e and C_e. R_e and C_e are both frequency dependent, making the overall impedance of the electrode (Z'_e) frequency dependent.

The amplifier's impedance (Z'_a) is also made up of several components. The amplifier itself has a complex input impedance (Z_a) that is frequency dependent (making the overall amplifier impedance frequency dependent). Shunt resistance R_{sh} and shunt capacitance C_{sh} represent the signal paths to ground through the electrode insulation and wire insulation. They can lower the effective amplifier impedance (Z'_a), causing measurement errors. The signal at the amplifier (V_{in}) can be filtered using hardware or software filters (represented by the transfer function $H(\omega)$). The post-filter recorded signal is represented by V_{rec}.

The equivalent circuit functions as a voltage divider. The recorded signal can be represented by the equation:

$$V_{rec} = H(\omega)V_{in} = H(\omega)\frac{V_{sig}Z'_a}{Z'_a + Z'_e} \tag{3.1}$$

This equation and the equivalent circuit above can be used to help understand the electrical sources or measurement errors in extracellular recordings.

3.4 Extracellular recording errors

Extracellular recordings can be prone to errors that affect the measurement of the underlying electric fields generated by neurons. This section will describe both equipment-related and tissue-related sources of error.

The equipment used for extracellular recordings can cause many types of measurement errors. The electrodes, wires, or amplifiers can be responsible for attenuating, filtering, or distorting the signal. They can also introduce noise into the recorded signal.

The equivalent circuit and voltage divider equation (Equation 3.1) help explain the origin of these errors. The extracellular recording accurately measures the underlying signal ($V_{rec} \simeq V_{sig}$) when the amplifier impedance is very large relative to the electrode impedance ($Z'_a \gg Z'_e$). If the magnitude of the amplifier impedance is not much larger than the electrode impedance, the recorded signal will be attenuated. This can also be a frequency-dependent effect, causing high-pass filtering. Also when the amplifier impedance is not large enough relative to the electrode impedance, the phase difference of the amplifier and electrode impedances can cause a distortion of the recorded signal. For this reason, amplifier input impedances should be very large. Otherwise, significant recording errors can occur, such as the frequency-dependent attenuation and phase shifting of local field potentials shown by Nelson et al. (2008). Similarly, because shunt capacitances can cause a reduction in the effective amplifier impedance, wires connecting the electrode to the amplifier should be kept short and well insulated.

Noise in the recording can also be minimized with some equipment considerations. To minimize thermal noise (also called Johnson noise), which is a function of resistance, the impedance of the electrode should be minimized. Additionally, to minimize interference and external noise sources (such as $60\,\mathrm{Hz}$ noise), the electrode impedance and shunt capacitances should be minimized. In Chapter 4, I will introduce a novel ultralow-impedance nanotexture coating for extracellular microelectrodes to minimize these noise sources.

When a foreign body, such as an extracellular recording electrode, is inserted inside the brain of a living animal, the damaged tissue in the brain and the tissue response can create significant problems for extracellular recordings. The response of the tissue has a complex time course and mechanism and has been well studied (Turner et al., 1999; Polikov et al., 2005). One of the many phases of the tissue response involves glia encapsulating the microelectrode. This encapsulation tissue has a very high impedance and can cause the impedance of the electrode-electrolyte interface to increase in the days and weeks after surgery (Williams et al., 2007). The magnitude of tissue response can be affected by electrode-insertion methods (Stice and Muthuswamy, 2009) and implant geometry (Edell et al., 1992). Biocompatible materials and coatings (Williams, 2008) and localized drug delivery (Onuki et al., 2008) can also be used to reduce the severity of the tissue response. In Chapter 6, I will show how design considerations in biocompatible materials and implant geometry can be used in order to minimize tissue damage when packaging an implantable device.

Chapter 4

Nanotextured coatings for ultralow impedance microelectrodes

Parts of this chapter have been previously reported in Ferguson et al. (2009).

4.1 Preparing tetrodes

As described in Chapter 3, stereotrodes and tetrodes are a powerful tool for recording extracellular signals from neural ensembles in freely moving animals. Stereotrodes (McNaughton et al., 1983) are made by spinning two insulated wires together, heating the insulation so it melts and the two wires join together, and cutting the tips of the wires to expose the microelectrodes (Figure 4.1). Tetrodes (Wilson and McNaughton, 1993; O'Keefe and Recce, 1993; Gray et al., 1995) are bundles of four microwires and are prepared in a similar manner to stereotrodes.

Because tetrodes are much more commonly used today than stereotrodes in neuroscience research labs, including in our lab, the remainder of this chapter will focus on tetrodes. However, the same principles and techniques can be applied to stereotrodes or single wire microelectrodes.

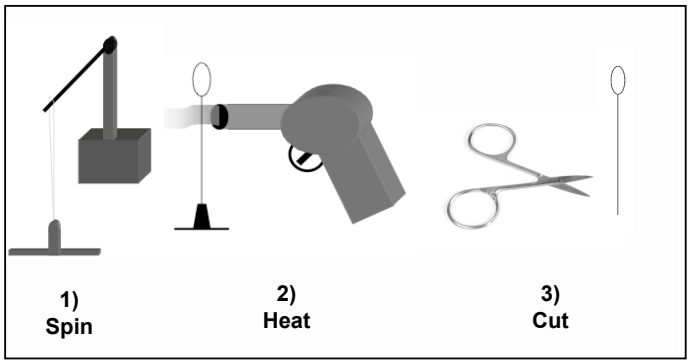

Figure 4.1: *Steps in preparing a stereotrode or a tetrode. Clipart from neuralynx.com.*

Cutting the ends of the microwire bundles with scissors seems like a straightforward step in the production of tetrodes, but it can be problematic. In the Redish Lab, we have found inherent variation in the electrical properties and recording performance of tetrodes. A major contributor to this variation is the area of the electrodes exposed at the tips of a tetrode. Upon inspection in a scanning electron microscope, we noticed that many tetrodes were severely damaged by the scissors during cutting. This frequently resulted in irregular exposed areas on the elec-

trodes and insulation that is damaged or uneven. Figure 4.2 shows a tetrode cut using sharp (unserrated) scissors, which are standard for cutting tetrodes.

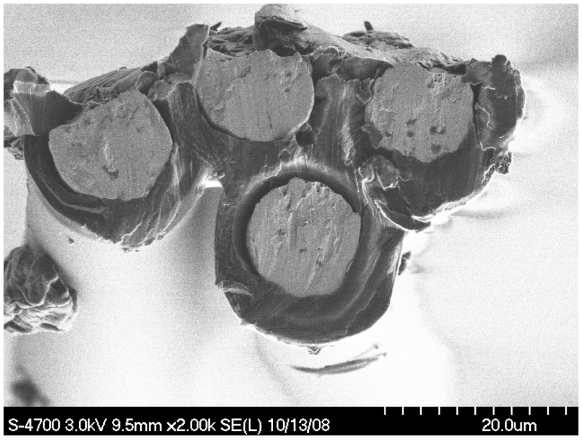

Figure 4.2: *Scanning electron microscope image of a poorly cut tetrode.*

As it turns out, this problem has occurred for almost two decades but has largely been unnoticed because a cleanly cut tetrode looks identical to a poorly cut tetrode under a standard microscope due to its small size. Only a scanning electron microscope, which is time consuming and expensive to use, reveals the extent of damage of the cut. A figure from the original paper describing stereotrodes McNaughton et al. (1983) showed a scanning electron microscope image of a damaged stereotrode that had been cut with sharp scissors. However, this damage was not commented upon in the paper, and the issue of scissors causing damage has not received much discussion since then.

In order to eliminate the damage to tetrodes caused by scissors, we tried cutting tetrodes using several different types of scissors and different cutting techniques. In the end, we found that tetrodes cut with serrated blade scissors resulted

in clean and level cuts with minimal damage to the insulation (Figure 4.3). It was also important to place the microwire bundle in the bottom of a notch of the serrated blade (using a microscope) and to ensure the notch did not have any nicks or a misshapen edge.

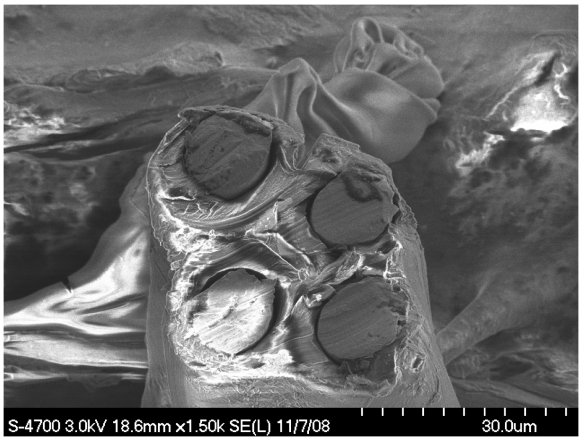

Figure 4.3: *Scanning electron microscope image of a tetrode with an improved cut and minimal damage. The white portion of the image is an artifact due to electrical charging of the substrate.*

4.2 Electroplating tetrodes

The impedances of tetrodes can greatly affect the quality of neural recordings (Robinson, 1968; Geddes, 1972). Because of small exposed area of the electrodes, freshly cut tetrodes have high impedances, which is associated with increased thermal noise and signal loss to shunt pathways (Loeb et al., 1995; Ludwig et al., 2006). In order to reduce the impedances, tetrodes are usually electroplated with gold or platinum.

Electroplating causes the deposition and growth of crystallites on the tips of tetrode microwires, increasing their effective surface areas and lowering their impedances. However, excessive electroplating of a tetrode can cause the crystallites on one microwire to grow too much and touch the crystallites on the other microwires, causing a short. Usually, tetrodes made from 10-to-30-μm diameter wires are plated to moderate impedance levels of 200–500 kΩ (at 1 kHz) because plating to below 100 kΩ results in shorting.

Tetrode recordings would benefit from a new method to lower impedances even further, allowing for the isolation of small-amplitude signals that were previously hidden by thermal noise or lost to shunt pathways, thereby enhancing sensitivity without sacrificing selectivity. Recently, several innovative methods have been developed to lower microelectrode impedances, including the use of conductive polymers (Ludwig et al., 2006), titanium nitride (Janders et al., 1996), iridium oxide (Cogan, 2008), and roughened polysilicon (Cui and Martin, 2003). However, these methods have not been tested on tetrodes and would be difficult for most neurophysiologists to recreate in their own labs without acquiring expensive new equipment. A more practical alternative would be to modify the standard electroplating process most neurophysiologists currently use. Cui and Martin (2003) showed that altering the concentration of gold-plating solution and electroplating current can change the morphology of a gold-plated microelectrode coating. Additionally, Keefer et al. (2008) found that adding multi-walled carbon nanotubes (MWCNTs) to a gold-plating solution created microelectrode coatings with a "rice-like" texture and very low impedances.

In the next few sections of this dissertation, I will report how we combined and expanded upon the methods of Cui and Martin (2003) and Keefer et al. (2008) and investigated how to create low-impedance coatings for tetrodes. This will largely follow Ferguson et al. (2009) but with additional unpublished results and figures included. As an overview, we start by examining tetrode coatings produced using various gold-plating solution concentrations and electroplating currents. Then, I will explain how we made tetrodes with the "rice-like" texture described by Keefer et al. (2008) using MWCNTs and made tetrodes with a similar texture using an additive not discussed in Keefer et al. (2008), polyethylene glycol (PEG). Additionally, I will describe a new coating with a very large surface area (made with MWCNTs or PEG and a low electroplating current) that consistently lowered the impedances of tetrodes to 30–70 kΩ without shorting. Finally, I will show that the low-impedance coatings improved recording quality in saline and *in vivo* tests.

4.2.1 Detailed electroplating methods

Gold-plated tetrodes were fabricated using standard methods (Wilson and McNaughton, 1993; Gray et al., 1995) with some modifications. Four 12.7-μm diameter, polyimide-insulated, nickel-chromium wires (Rediohm-800, Kanthal Precision Wire, Palm Coast, FL) were twisted together and heated to melt the insulation, creating a stiff bundle of four microwires. Tetrodes were carefully cut under a surgical microscope using micro-serrated, stainless-steel scissors (14054-13, Fine Science Tools, Foster City, CA). The tetrode tips were immersed in an electroplat-

ing solution made of non-cyanide, gold-plating solution (5355, SIFCO Selective Plating, Cleveland, OH) by itself or mixed with one of three additives: deionized (DI) water, a MWCNT solution (1 mg/mL in DI, less than 8 nm diameter, Cheap Tubes, Brattleboro, VT), or a PEG solution (1 mg/mL in DI, Sigma-Aldrich, St. Louis, MO). Sonication was used to help mix the solutions that contained MWCNTs. Tetrodes were electroplated with constant-current pulses from a stimulus isolator (A365D, World Precision Instruments, Sarasota, FL). The tetrode was also connected to a metal electrode impedance tester (IMP-1, Bak Electronics, Mount Airy, MD) that measured impedance at 1 kHz. A 1-s, reversed-polarity pulse helped to clean the surface of the tetrode tip and lowered the impedances to 2–3 MΩ before electroplating. Electroplating pulses were 1–5 s long and were repeated until the tetrodes reached the desired impedances. After electroplating, the tetrodes were soaked in DI, air dried, and checked for shorts.

Forty different sets of electroplating parameters (ten electroplating solutions and four levels of electroplating current) were tested to try to reduce the impedance of all four electrodes in a tetrode to below 100 kΩ without shorting. Nine electroplating solutions were made by mixing the three additives (DI, MWCNT, and PEG) with the gold-plating solution at three different concentrations: 25%, 75%, and 90% (percent volume of additive solution per total volume). The tenth solution was the gold-plating solution without additives. The four levels of electroplating current were 0.1 μA, 0.5 μA, 2 μA, and 5 μA. Many of the forty electroplating parameters were also used to electroplate tetrodes to 250 kΩ in order to study the resulting coatings at an impedance level that was less likely to cause shorting.

To observe the texture of the coatings, the tetrodes were attached to a brass mount and imaged in a field-emission scanning electron microscope (S-4700, Hitachi, Tokyo, Japan). Electrical impedance spectroscopy was performed with 5 mV applied AC signals using a potentiostat (Reference 600, Gamry Instruments, Warminster, PA), a platinum counter electrode, and a silver silver-chloride electrode.

Saline and *in vivo* tests were conducted to investigate the quality of recordings using low-impedance tetrode coatings. Tetrodes were electroplated so that at least two of the four electrodes within each tetrode had different impedances (measured at 1 kHz), allowing for comparisons of simultaneously recorded signals within the same tetrode. For the saline test, a tetrode was inserted 3 mm deep into a phosphate-buffered saline bath to record background noise levels. For the *in vivo* tests, background and neural signals were recorded from thirteen distinct locations with spiking activity in two anesthetized rats (Brown Norway-Fisher 344 hybrid, Harlan, IA, USA) using four different tetrodes. Six of the thirteen recordings locations were found while listening to spiking activity on standard-impedance electrodes, and the rest while listening to low-impedance electrodes.

For both the saline and *in vivo* recordings, signals were referenced to ground and connected to a high-input-impedance, low-noise amplifier (Model 1700, A-M Systems, Sequim, WA) by driven-shield cables. Recordings were performed in a grounded Faraday cage and on a vibration isolation table. Signals were recorded with 1000x gain with the amplifiers filters set from 1 Hz to 10 kHz and without a notch filter. The amplified signal was sampled at 32 kHz using LabVIEW and

a data acquisition card (PCI-6251, National Instruments, Austin, TX) and analyzed in MATLAB (The MathWorks, Natick, MA). Rats were anesthetized with Nembutal (sodium pentobarbital, 50 mg/kg, Abbott Laboratories, North Chicago, IL) and maintained using isoflurane (0.5–2.0% isoflurane vaporized in medical grade oxygen) during recordings. Recordings were taken from both cortex dorsal to hippocampus and hippocampus (anteroposterior -3.8 mm and mediolateral 2.5 mm from bregma). All procedures were in accordance with National Institutes of Health guidelines for animal care and approved by the Institutional Animal Care and Use Committee (IACUC) at the University of Minnesota.

4.2.2 Electroplating results

Standard gold electroplating of tetrodes

Before electroplating, tetrode tips resembled four flat, slate-like circles surrounded by insulation (Figure 4.4A) and had electrode impedances of 2–3 MΩ. Tetrodes that were electroplated to 250 kΩ using standard parameters (2 μA current pulses and an unmodified gold-plating solution) had an uneven, granular coating of gold crystallites with larger crystallites near the outside edges (Figure 4.4B). All attempts to lower the impedance of the four electrodes in a tetrode to below 100 kΩ using standard electroplating parameters resulted in shorting. Varying the electroplating current and concentration of gold-plating solution using DI (no other additives) also resulted in shorting.

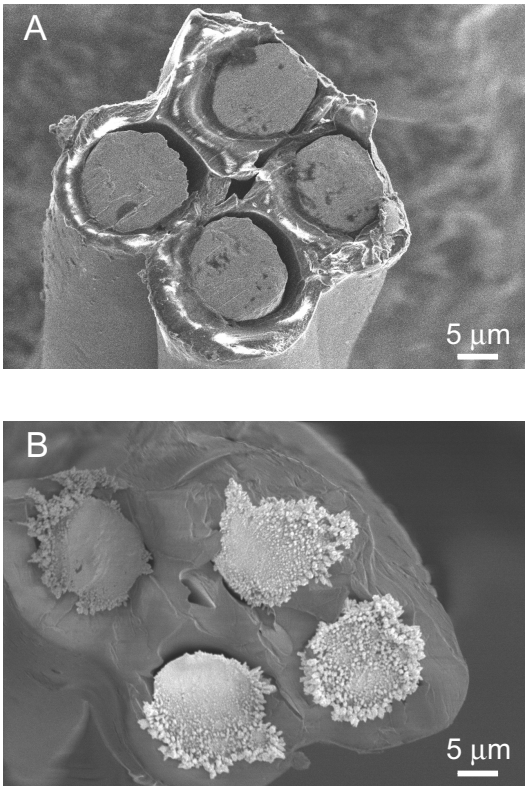

Figure 4.4: *Scanning electron microscope images of a tetrode (A) before electroplating and (B) after electroplating to 250 kΩ using an unmodified gold-plating solution. Figure from Ferguson et al. (2009).*

Creating a "rice-like" texture

Within the set of forty different electroplating parameters, a wide variety of coating textures were created. One set of electroplating parameters, 2 μA current pulses and the 90% multi-walled carbon nanotube (MWCNT) solution, was able to consistently produce 250kΩ tetrodes with the same "rice-like" texture as described by Keefer et al. (2008) (Figure 4.5A). Closer examination revealed the texture contained bladed crystallites (Figure 4.5B). The 90% polyethylene glycol (PEG) solution produced a similar bladed texture (Figure 4.5D), but the crystallites had uneven growth across the electrodes and appeared less "rice-like" (Figure 4.5C). Coatings made with the 90% deionized (DI) water solution were much flatter (Figure 4.5E) and had a small amount of bladed crystallite growth (Figure 4.5F). All attempts to lower tetrodes impedances to below 100kΩ after adding 90% MWCNT, 90% PEG, or 90% DI to the gold-plating solution resulted in shorting.

Electroplating to below 100 kΩ

Without additives, all tetrodes shorted when plated to below 100 kΩ. However, at 250 kOhms, the tetrodes displayed a variety of coating types. Figure 4.6 shows 16 different electrodes that were made using four ratios of DI and standard gold plating solution and four different levels of current pulses. Figure 4.7 shows a zoomed in view of these different coating textures.

Only two of the forty sets of electroplating parameters tested were able to con-

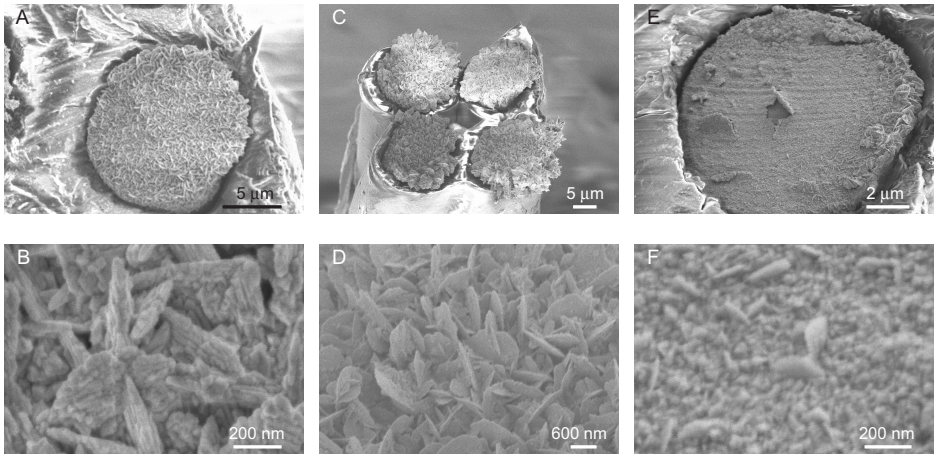

Figure 4.5: *(A) Tetrodes with "rice-like" coating and impedances of about 250 kΩ were made by electroplating with a 90% MWCNT solution and 2 µA current pulses. (B) A high-magnification image shows that the "rice-like" coating was made up of bladed crystallites. (C) Tetrodes with a similar coating and an impedance of about 250 kΩ were made by electroplating with 90% PEG solution and 2 µA current pulses. (D) The texture of this coating was also made up of bladed crystallites. (E) A much flatter, 250 kΩ coating was made by electroplating with a 90% DI solution and 2 µA current pulses. (F) This coating texture contained only a few bladed crystallites. Figure from Ferguson et al. (2009).*

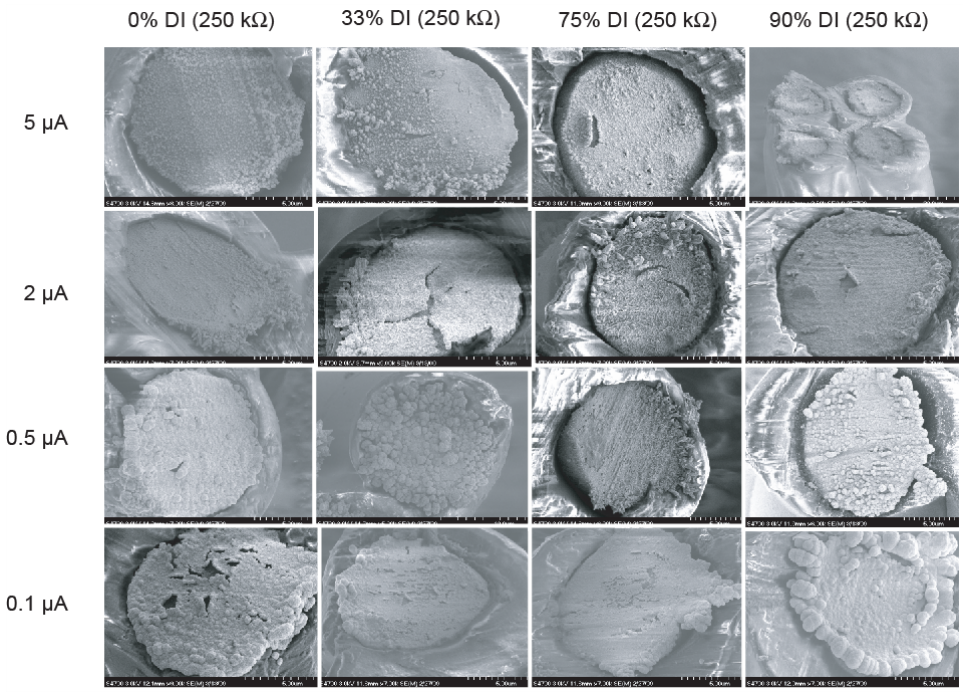

Figure 4.6: *Scanning electron microscope images of tetrodes that were electroplated to 250 kΩ without the use of additives. Only mixtures of deionized water and standard gold plating solution were used. Further electroplating to below 100 kΩ resulted in shorts for all sixteen sets of electroplating parameters.*

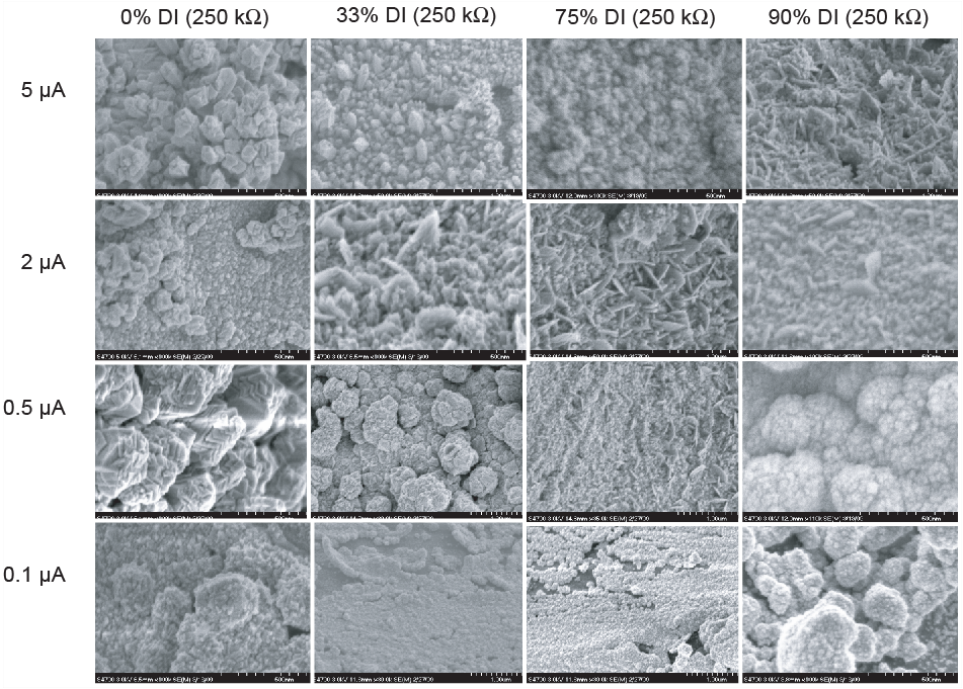

Figure 4.7: *A zoomed in view of the coating textures of the sixteen tetrodes from Figure 4.6.*

sistently produce tetrodes with impedances below 100 kΩ without shorting: the 75% PEG and the 75% MWCNT solutions, both using 0.1 μA current pulses. The coatings made with the 75% MWCNT solution had a globular appearance (Figure 4.8A) and a rough, large surface area texture (Figure 4.8B). The coatings from the 75% PEG solution were also globular and rough at high-magnification but grew large around the perimeter of the electrodes (Figure 4.8C and Figure 4.8D). Tetrodes with impedances as low as 30 kΩ were produced using these two sets of electroplating parameters.

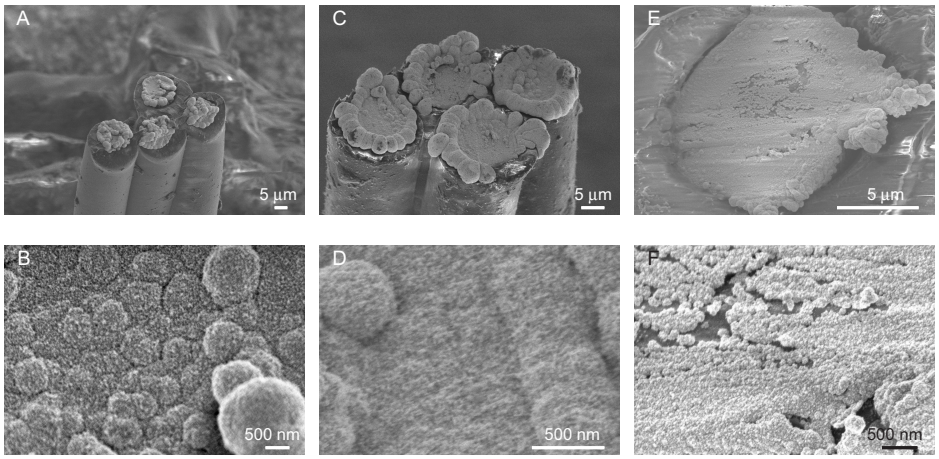

Figure 4.8: *(A) Tetrodes with globular coatings and impedances of 40–70 kΩ were made by electroplating with a 75% MWCNT solution and 0.1 μA current pulses. (B) The resulting coating texture was very rough. (C) Globular coatings with more peripheral growth but also with impedances of 4070 kΩ were made by electroplating with a 75% PEG solution and 0.1 μA current pulses. (D) The texture was also rough but had fewer globules than the coating made with the MWCNT solution. (E) A very different coating was made by electroplating with a 75% DI solution and 0.1 μA current pulses. Because these parameters caused tetrodes to short when plated below 100 kΩ, the coating shown was only plated to 250 kΩ. (F) This coating was only sparsely covered by crystallites. Figure from Ferguson et al. (2009).*

Without additives (using a 75% DI solution and 0.1 μA current pulses), tetrodes plated to below 100 kΩ were shorted. Figure 4.8E and Figure 4.8F show a tetrode plated to 250 kΩ using the 75% DI solution.

4.2.3 Electrical properties of the coatings

Electrical impedance spectroscopy was performed on two tetrodes that were electroplated to below 100 kΩ (using 75% MWCNT and 75% PEG solutions). Their impedance spectra were similar across frequencies (Figure 4.9A). At 1 kHz, the two tetrodes had impedances of 70 kΩ and phase angles of about -50°. These tetrodes were less capacitive than a standard gold-plated, 250-kΩ tetrode which had a -80° phase angle at 1 kHz (Figure 4.9B).

Saline test

A tetrode recording in a saline bath revealed that a low-impedance electrode had a smaller noise level than a standard-impedance electrode and an unplated electrode. Figure 4.10 shows a representative 1-s recording of three electrodes with different impedances on the same tetrode. The low-impedance electrode (30 kΩ) had an RMS noise level of 2.2 μV, the standard-impedance electrode (330 kΩ) of 3.0 μV, and the unplated electrode (2.5 MΩ) of 9.0 μV with a large 60-Hz noise component.

The noise levels of the saline recordings were similar to estimates of the expected thermal noise. Because the electrodes had a frequency-dependent complex

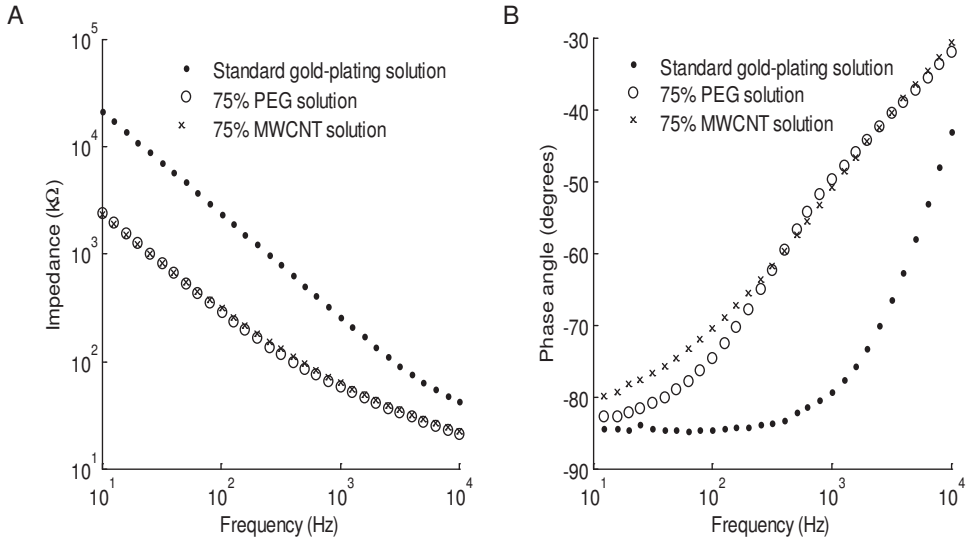

Figure 4.9: *Electrical impedance spectroscopy of the tetrodes electroplated to 70 kΩ (using 75% MWCNT and 75% PEG solutions) compared with tetrodes plated to 250 kΩ (using unmodified gold-plating solution). (A) The impedances of the tetrodes made with the 75% MWCNT and PEG solutions were almost identical and were lower than the impedances of the tetrodes made with the unmodified gold-plating solution, across all frequencies. (B) The low-impedance tetrodes were much less capacitive than the tetrodes plated with unmodified gold-plating solution, as measured by phase angles. Figure from Ferguson et al. (2009).*

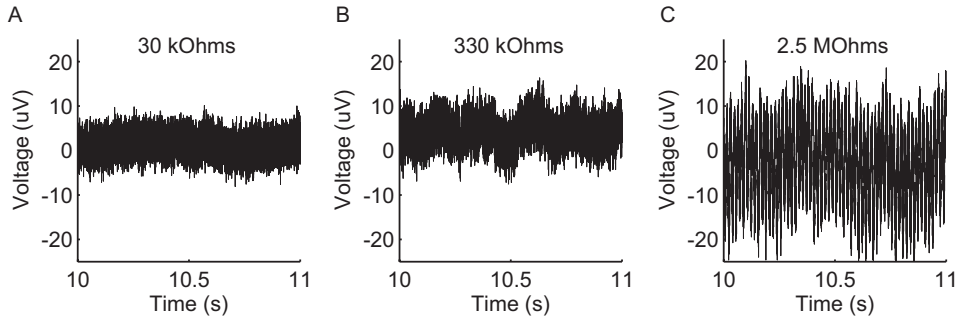

Figure 4.10: *Simultaneous recordings in saline of three electrodes with different impedances on the same tetrode. The low-impedance electrode (30 kΩ) had an RMS noise level of 2.2 μV, the standard-impedance electrode (330 kΩ) of 3.0 μV, and the unplated electrode (2.5 MΩ) of 9.0 μV with a large 60 Hz noise component. The 1-s sample shown was similar to the rest of the recording. Figure from Ferguson et al. (2009).*

impedance, RMS thermal noise was estimated as:

$$V_{rms} = \sqrt{\sum_{freq.} 4kTR\Delta f} \tag{4.1}$$

where k is Boltzmanns constant, T is temperature, R is the real component of the complex impedance at a given frequency, and Δf is the frequency difference between impedance measurements. Using 40 impedance values measured at frequencies between 1 Hz and 10 kHz, the thermal noise of the low-impedance electrode (30 kΩ) was estimated to be 1.5 μV, a standard-impedance electrode (330 kΩ) was 3.3 μV, and an unplated electrode (2.5 MΩ) was 8.3 μV.

***In vivo* test**

Tetrode recordings in anesthetized rats were sensitive to the impedance of the electrodes. Four tetrodes were used to record signals in thirteen distinct locations with spiking activity in two anesthetized rats. Three tetrodes had impedances of 50 kΩ, 50 kΩ, 250 kΩ, and 250 kΩ. The fourth tetrode had impedances of 50 kΩ, 270 kΩ , 2.5 MΩ, and 2.5 MΩ. When the signals were filtered from 1 Hz to 475 Hz in MATLAB to look at local field potentials, the low-impedance electrodes (50 kΩ) consistently recorded approximately 20% larger signals than standard-impedance electrodes (250 kΩ) with no noticeable difference in frequency content (Figure 4.11A).

When the signals were filtered from 600 Hz to 6 kHz to observe spiking activity, the RMS background noise levels between spiking events were slightly larger

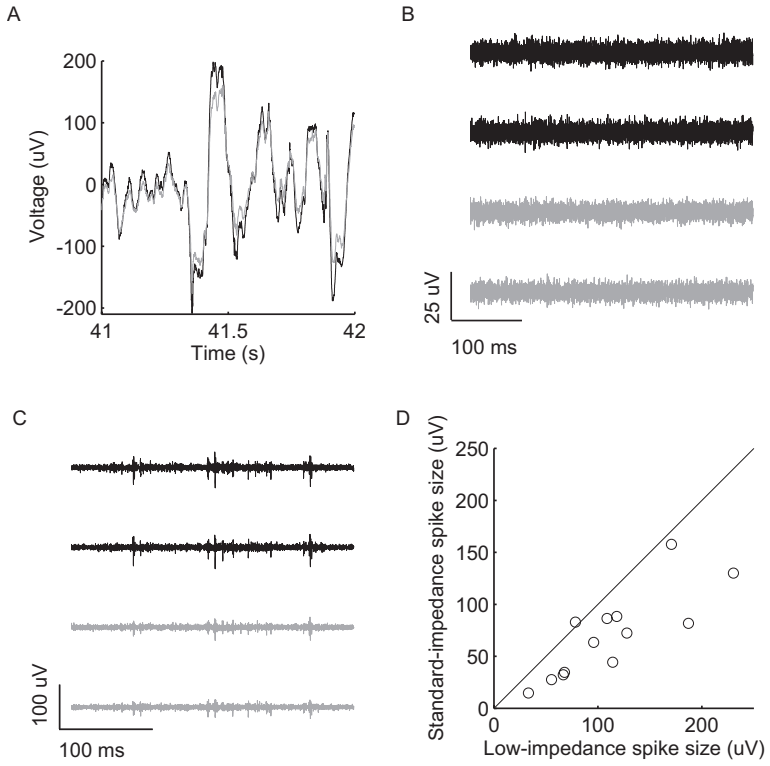

Figure 4.11: In vivo *recordings using tetrodes that contain both low-impedance(∼50 kΩ) and standard-impedance (∼250 kΩ) electrodes. (A) Low-impedance electrodes recorded approximately 20% larger local field potentials (filtered from 1 Hz to 475 Hz) than standard-impedance electrodes. The 1-s sample shown was from the middle of the recording and was representative of the rest of the recording. (B) A background recording (filtered from 600 Hz to 6 kHz) without large spikes. The black traces were from the low-impedance electrodes on the tetrode, and the gray traces were from the standard-impedance electrodes. The RMS background level was 2.7 μV for low-impedance electrodes and 2.5 μV for standard-impedance electrodes. (C) A tetrode recording with spikes shows that the amplitudes of the spikes were larger on the low-impedance electrodes than the standard-impedance electrodes. (D) In twelve of the thirteen recording locations, the largest spike seen on any electrode had larger mean peak-to-peak amplitudes on the low-impedance electrodes than on the standard-impedance electrodes. Figure from Ferguson et al. (2009).*

in the low-impedance electrodes (2.7 μV) than standard-impedance electrodes (2.5 μV) (Figure 4.11B). The reduction in thermal noise seen in the saline tests was obscured by other forms of noise, such as small action potentials from distant neurons or capacitively coupled interference (e.g., from power lines, nearby electrical equipment, or lights). Another benefit of the low-impedance electrodes was a better impedance match to the already-low-impedance reference electrode, which improved the common-mode rejection ratio.

Additionally, the peak-to-peak amplitude of spikes was generally larger on low-impedance electrodes than on standard-impedance tetrodes within a tetrode. Figure 4.11C shows one example. For the largest spike seen on any electrode at each of the thirteen recording locations, the mean amplitude of the spike on the low-impedance electrodes was compared to the mean amplitude of the same spike on the standard-impedance electrodes. In twelve of the thirteen locations, the amplitudes of the spikes were larger on the low-impedance electrodes than the standard-impedance electrodes (Figure 4.11D). One very large spike recorded at one of the locations was excluded from this graph because it only occurred twice during the 2 min recording, and the second largest spike was used instead. However, the excluded spike also had a larger-amplitude spike on the low-impedance electrodes. The presence of larger-amplitude spikes on the low-impedance electrodes was not dependent on whether low-impedance or standard-impedance spikes were used to listen for spiking activity while turning the tetrodes.

4.2.4 Discussion of electroplating results

Electroplating is a simple yet powerful technique that is not used to its full potential by most neurophysiologists who electroplate their own microelectrodes. Commercial plating solutions designed for industrial applications are often used straight out of the bottle to electroplate tetrodes. However, by mixing additives with the electroplating solution and varying other electroplating parameters, neurophysiologists can easily create a variety of coatings with different crystallite shapes, sizes, and densities.

We used electroplating additives to produce several distinct tetrode coatings, most notably globular coatings with a very large surface area and coatings with the "rice-like" texture described by Keefer et al. (2008). Tetrodes with the globular coatings could reach impedances of 30–70 kΩ without shorts and had a less negative phase angle than standard 250 kΩ tetrodes. Coatings with a bladed texture could be produced using either multi-walled carbon nanotubes (MWCNT) or polyethylene glycol (PEG) solutions, implying that the coating was not created by the deposition of non-dispersed bundles of carbon nanotubes as suggested by Keefer et al. (2008). Rather, we believe the MWCNT and PEG additives acted as electroplating inhibitors, which adsorbed to electrode surfaces and changed the dynamics of electrocrystallization to favor the deposition of new crystallites over continued growth of existing crystallites (Feltham and Spiro, 1971; Lin et al., 1986; Winand, 1994). PEG is a known electroplating inhibitor (Stoychev and Tsvetanov, 1996), and the coatings produced with MWCNTs and PEG were sim-

ilar but not identical because the molecules are different sizes and likely have different strengths of inhibition. Coatings made with inhibitors have other benefits, such as increased adhesion to the substrate (Weil, 1989). Merrill and Ainsworth (1972) found that adding gelatin to a platinum plating solution increased the adhesion of the platinum coating to tungsten microelectrodes. A downside of using electroplating inhibitors is that electroplating a single tetrode to below 70 kΩ can take up to 20 min, as opposed to the 1–2 min needed to electroplate a single tetrode to 250 kΩ without inhibitors.

We found that the low-impedance tetrode coatings reduced the thermal noise measured in a saline test, but this noise reduction was weaker in an *in vivo* recording. To test how the impedance of the electrodes changed over time, six tetrodes were implanted in the striatum of a rat and six tetrodes were implanted in the Hippocampus. Each tetrode had two electrodes that were plated to approximately 250 kΩ and two that were plated to below 100 kΩ. The impedances of all the tetrodes rose after insertion and continued to rise for the next week or two. After about 10 days, the impedances either plateaued or reduced to a lower level. Overall, the impedances of all tetrodes rose after implantation, and the average impedances of the electrodes that started below 100 kΩ continued to be less than the electrodes that began at impedances of approximately 250 kΩ. However, there was significant variability in the impedances of each tetrode due to the complex nature of the local tissue response and electrode encapsulation, which were not present in the anesthetized rat tests. In the *in vivo* recordings in anesthetized rats, the low-impedance electrode coatings significantly minimized signal loss through shunt

pathways and resulted in a larger signal for local field potential and for spikes.

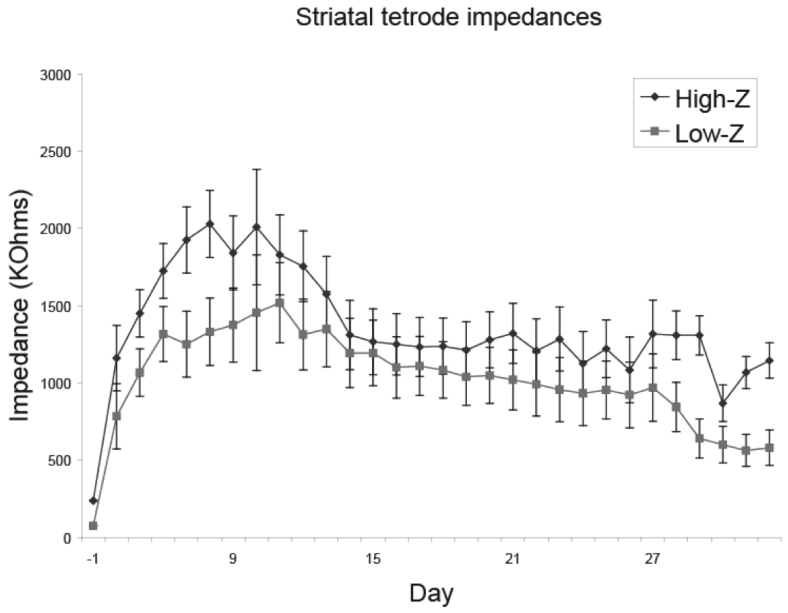

Figure 4.12: *Impedances of tetrodes implanted in the striatum over time. The upper line ('High-Z') corresponds to a tetrode electrodes that were plated to a standard impedance of approximately 250 kΩ before implantation (on Day -1). The lower line ('Low-Z') corresponds to tetrode electrodes that were plated to below 100 kΩ before implantation.*

There is conflicting evidence about whether microelectrodes with very low impedances improve the quality of chronic *in vivo* neural recordings. Some studies have found that low-impedance microelectrodes improved recordings while others did not find a significant difference. One study found that low-impedance coated microelectrodes recorded 17% more quality units and also reduced low-frequency (0.1–1 Hz) artifacts over six weeks post-implantation (Ludwig et al., 2006). Another long-term study was able to record neural activity with a high signal-to-noise ratio (SNR) using microelectrodes with impedances ranging from 50 kΩ to 1 MΩ

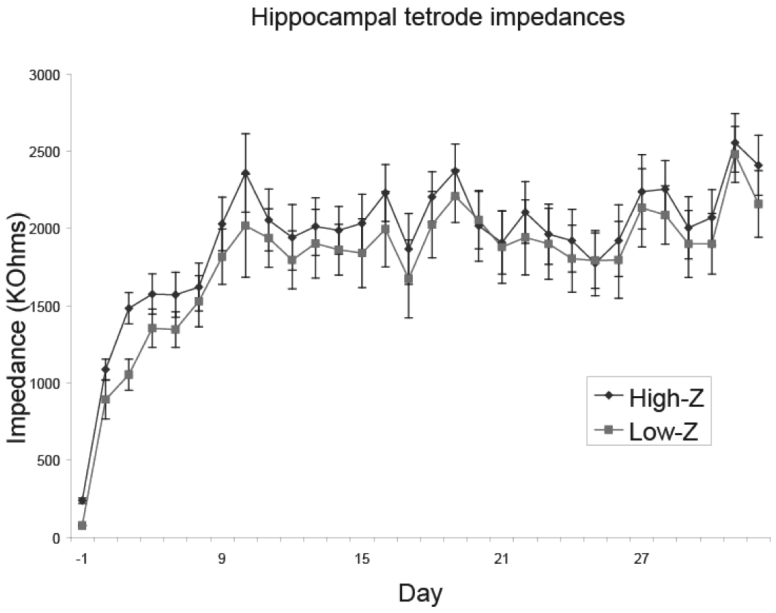

Figure 4.13: *Impedances of tetrodes implanted in the Hippocampus over time. The upper line ('High-Z') corresponds to tetrode electrodes that were plated to a standard impedance of approximately 250 kΩ before implantation (on Day -1). The lower line ('Low-Z') corresponds to tetrode electrodes that were plated to below 100 kΩ before implantation.*

and suggested that low impedances were not necessary for high-SNR recordings (Suner et al., 2005). This study also found that SNR and impedance were significantly correlated for one animal but not for another animal, while signal quality and impedance were significantly correlated for both animals. These results are in agreement with previous studies that showed a large amount of animal-to-animal variation in the type and magnitude of the tissue response to chronic implants (Polikov et al., 2005; McConnell et al., 2009).

In addition, some regions of the brain, such as the cerebellum, have a high density of neurons and are not well suited to low impedance recordings. The low impedance microelectrodes would pick up many simultaneous signals that would be difficult to separate, resulting in a difficult analysis. A high impedance microelectrode would increase the specificity of recording by picking up the extracellular signals from one neuron. But on the other hand, the high impedance of the electrode could cause a distortion in the waveform, increase the background thermal noise, and reduce the number of simultaneously recorded neurons in an ensemble.

To help illustrate this tradeoff, imagine recording a conversation at a cocktail party. When the party begins and there are very few people in the room, it is easy to hear and distinguish the voices of multiple people in a conversation. A single microphone could be used to record everyone. Listening to the recording later, the voices and words of the individual speakers could be easily separated. However as the room gets more crowded, it becomes increasingly difficult to hear any single speaker. The background signal (room noise) becomes overwhelming causing

people to lean in closer or cup their ears to hear better. If a single microphone were to be used, it would only pickup a loud buzz of voices and no individual speakers. Alternatively, a more directionally selective, less sensitive microphone placed closer to individual speakers would allow for a recording in a crowded party. Thus, different environments, both in a cocktail party and in the brain, have different listening/recording requirements.

Neurophysiologists interested in testing whether low-impedance tetrodes work for their specific research application can conveniently do so by using electroplating additives. However, as mentioned, these low-impedance tetrodes take longer to prepare and may not work for all applications. We found that MWCNT solutions created more compact coatings than PEG when viewed in a scanning electron microscope, but PEG is more commonly found in neurophysiology labs and was equivalently effective at lowering impedances. Electroplating is simple to perform yet has great flexibility and can be modified to create coatings with a wide variety of properties. In addition to the electroplating parameters varied in this study (additives, plating current, and plating solution concentration), many other variables can influence the electroplating process (e.g., pH, stirring, pulse timing, and temperature). Electroplated microelectrode coatings can be made to have a range of properties, and their usefulness for neural recording applications is only starting to be explored.

Chapter 5

Nanoelectrodes for intracellular neural recordings

Parts of this chapter follow Ferguson et al. (Under review).

5.1 Previous state of the art

Intracellular recordings are widely used by biomedical researchers to investigate the biophysical dynamics of neurons and can reveal changes in membrane potentials that reveal both the synaptic inputs and action potential output signals of neurons. Typically, a glass micropipette with a tip diameter on the order of 0.1–1 μm is used to perform intracellular recordings (Purves, 1981). A sharp electrode has an open tip and large shaft that penetrate the neuronal membrane as it gains access to the inside of the cell. This action causes cell damage and ionic leakage that af-

fects the fidelity of the recording and eventually limits the duration of recording to a few hours or less. A patch electrode can also dialyze a cell by replacing the cells cytoplasm with the fluid inside the micropipette, limiting recording time across cell membranes and contributing to eventual cell death (Hamill et al., 1981).

Nanoelectrodes with tip diameters considerably less than 1 µm have the potential to minimize membrane damage during cell penetration, thus allowing for long-duration intracellular recordings. Furthermore, multielectrode array (MEA) devices, which are currently limited to extracellular recordings, can use nanoelectrodes to create new ways of recording chronically across cell populations. Ideally, a nanoelectrode should have a diameter of less than 100 nm as cells have been shown to have significantly shorter survival times with larger diameter nanowires (Kim et al., 2007). Nanoelectrodes with nanoscale tip diameters able to obtain intracellular membrane potential recordings have been fabricated with silicon nanowires (Tian et al., 2010), carbon nanopipettes (Schrlau et al., 2009), highly polished glass nanopipettes (Sun et al., 2008), and sharpened silicon needles (Hanein et al., 2002). However, after insertion, the portion of the electrode in contact with the membrane is often much larger than 100 nm due to the kinked design of the nanowires or the taper of the nanopipettes and needles. To minimize the contact area with a cell membrane, de Asis et al. introduced a nanoelectrode that had a high aspect ratio using a single multiwalled carbon nanotube to penetrate a cell (de Asis et al., 2009). Its support structure, however, was large and not suited for recording from neurons deep within complex neural tissues, such as in brain slices or the intact brain, where the electrodes must pass through several

tens or hundreds of microns of tissue before reaching their target neurons.

In this chapter, I will present a novel approach to fabricating nanoelectrodes that addresses these challenges and limitations, and demonstrate that our design permits the intracellular recording of action potentials within rat brain slice and a leech ganglion. We developed a three-step process to construct our high aspect ratio nanoelectrodes: (1) nanowires were grown on the end of traditional microwire electrodes using electron-beam-induced deposition (EBID), (2) the nanowires were completely insulated using atomic layer deposition (ALD), and (3) the insulation was removed from the tips with a focused ion beam (FIB).

5.2 Materials and Methods

In developing the nanoelectrodes, we investigated numerous designs and fabrication methods. In order to better understand how we arrived at our final successful design, I will describe some of the unsuccessful methods of creating nanoelectrodes (Figure 5.1).

One unsuccessful approach to growing nanowires was using template synthesis. In this technique, gold and other metal nanowires can be grown by electroplating through a porous membrane with pore diameters of tens of nanometers and then removing the membrane, leaving a forrest of vertical nanowires (Schönenberger et al., 1997). We tried this technique using polycarbonate membranes pushed firmly against the end of an insulated tetrode. We electroplated gold and then dissolved the polycarbonate membrane using chloroform. However, be-

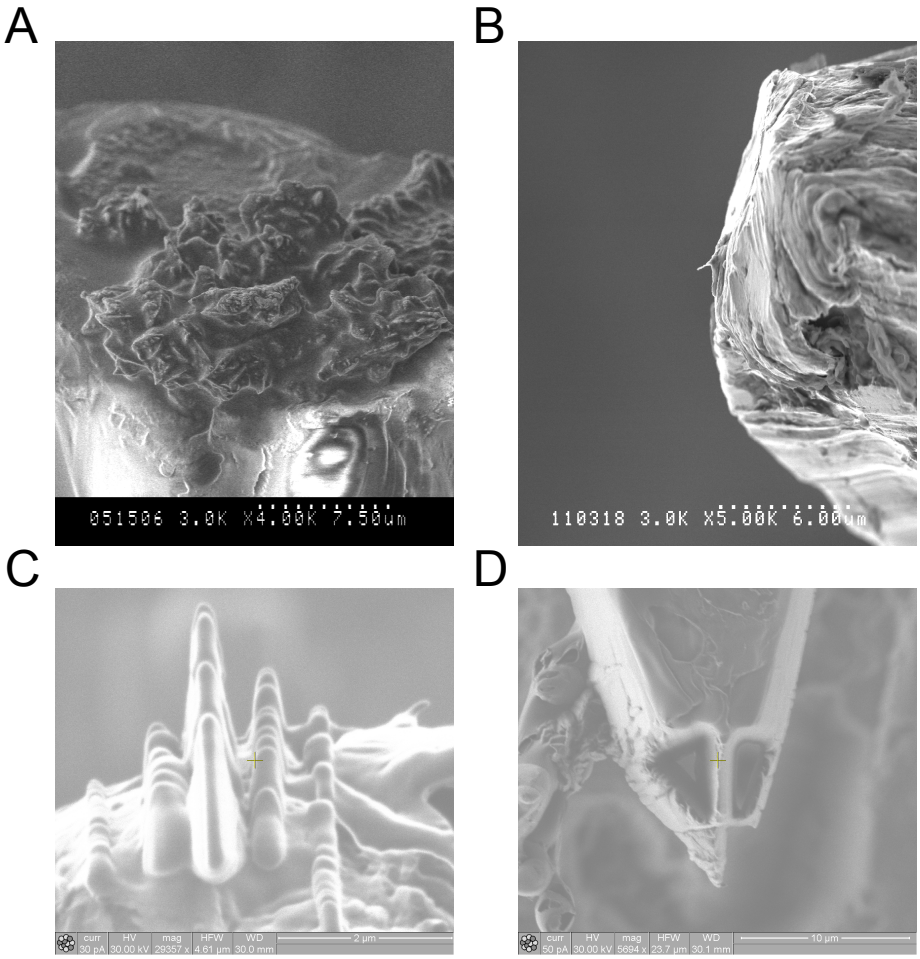

Figure 5.1: *Scanning electron microscope images of four unsuccessful methods of growing nanowires. (A) Instead of gold nanowires, gold blobs were grown when a tetrode was electroplated with a nanoporous polycarbonate filter on top. (B) Nanowires grown using Electron Beam Induced Deposition (EBID) looked promising in scanning electron microscope images but had very large values of shunt capacitance. (C) Attempts to grow nanowires using Ion Beam Induced Deposition (IBID) resulted in rows of nanowires on top of each other. (D) A subtractive approach using Focused Ion Beam milling took over an hour per nanowire and did not completely mill through the thickness of a microwire.*

cause the membrane was not completely attached to the tetrode, the electroplating caused the gold to push up the membrane and resulted in gold blobs on the surface of the tetrode (Figure 5.1A).

A second unsuccessful technique used Electron Beam Induced Deposition (EBID) to grow nanowires on an uncoated silver wire. This approach resulted in nanowires that looked good in scanning electron microscope images (Figure 5.1B). However, because there was no insulation initially on the silver wire, the shunt capacitance was very large. This shunt capacitance caused a reduction in the effective amplifier impedance, meaning we were unable to record any neural signals because they were completely attenuated (see Section 2.2.1).

A third unsuccessful technique used Ion Beam Induced Deposition (IBID) to grow nanowires. This approach would allow for easy, programmable deposition of nanowires in the FEI Quanta 200 3D in the Nanofabrication Center at the University of Minnesota. However, the ion beam re-rastered multiple times for each attempted nanowire. This caused multiple nanowires to be grown on top of each other, effectively creating a pile of nanowires (Figure 5.1C). Attempts to make the the machine raster only once were unsuccessful.

A fourth unsuccessful technique used a subtractive approach to create nanowires, rather than growing them. In this approach, we tried using a Focused Ion Beam (FIB) to mill the end of a microwire to form a nanowire. We programmed spatial patterns for the FIB to remove two triangles of material from the tip, leaving a nanoscale column of material (Figure 5.1D). Then, we could rotate the microwire by 90° and mill two more triangles to create the nanostructure. However, this

approach was extremely time consuming, requiring well over an hour to produce one wire. Attempts to reduce the time, by increasing the beam current resulted in very rough cuts of the metal microelectrode. The roughness of the surfaces of the cut microelectrode was larger than the nanowires that we wanted to grow.

The final (and successful) procedure used to make the nanoelectrodes is shown on Figure 5.2. For the support structure, we chose to use traditional microelectrode recording microwires (18 μm in diameter and made of 90% platinum/10% iridium and insulated with polyimide; California Fine Wire, Grover Beach, CA). This microwire is routinely used to penetrate through intact rat brains in vivo to perform extracellular recordings of neurons for up to several months (McNaughton et al., 1983). To form the support structure for the nanoelectrode, a segment of microwire with a length of approximately 7 mm was cut with surgical scissors under a stereo microscope. One end was cut at a bias to an angle of about 20 degrees from vertical to allow for easier visualization from above in the scanning electron microscope (Figure 5.3A and Figure 5.3B).

As mentioned above, nanowires were grown using electron-beam-induced deposition (EBID), where a beam from an ultra-high resolution field-emission scanning electron microscope (S900, Hitachi, Tokyo, Japan) was focused on the end of the microwire and slowly scanned in horizontal lines extending out from the conductive portion of the microwire tip. No lithographic masks were necessary. Each EBID line scan took about one minute and created a wire with a diameter of 10–30 nm and a length of up to 2 microns (Figure 5.3C). This step was repeated until the desired number of nanowires was obtained. EBID was cho-

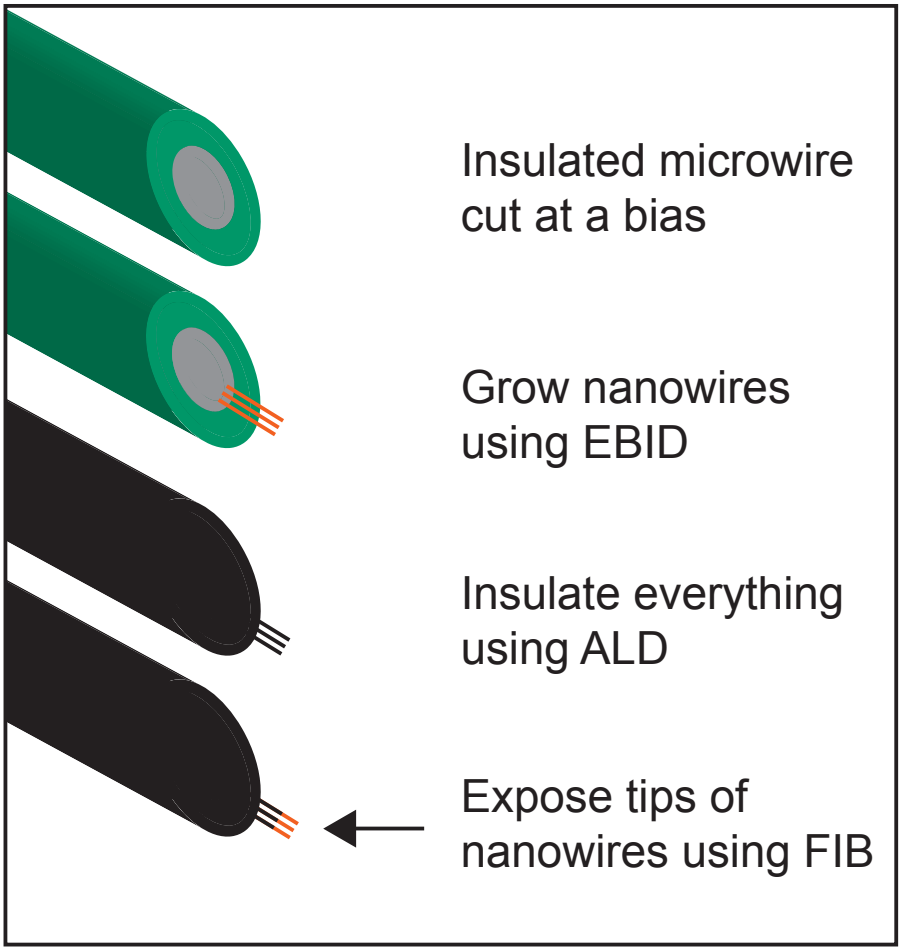

Figure 5.2: *Successful fabrication steps for the nanoelectrode. From Ferguson et al. (Under review).*

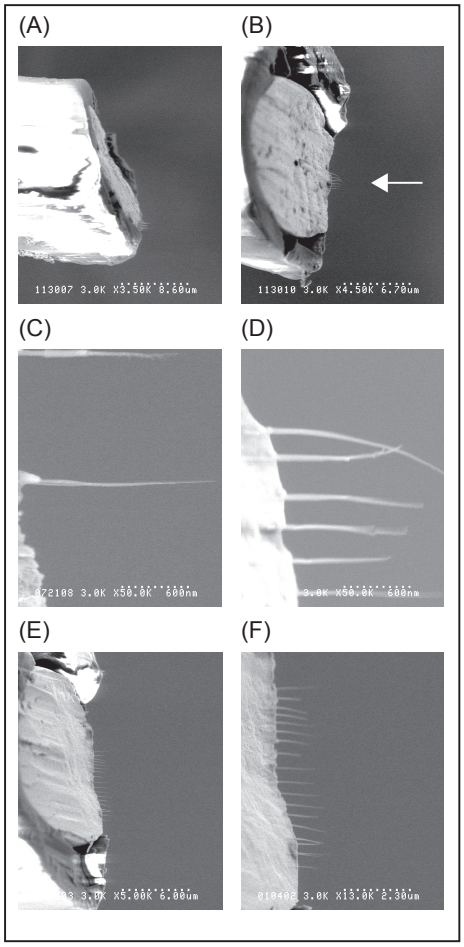

Figure 5.3: *Scanning electron microscope images of the fabricated nanoelectrode. (A) A side-view of a nanoelectrode shows the bias cut. (B) Nanoelectrodes were viewed from above during EBID growth of nanowires (shown with an arrow). (C) Single nanowires were grown using horizontal line scans. (D) Typically, six nanowires were grown per nanoelectrode. (E) As many as 18 nanowires were grown on a single nanoelectrode. (F) A closer view of the 18-nanowire nanoelectrode. From Ferguson et al. (Under review).*

sen because of its customizability; the length, number, and spacing of nanowires could be controlled for each nanoelectrode. Typically, six parallel nanowires were grown on the end of each nanoelectrode, reducing the impedance to the range of typical extracellular microwire electrodes (Figure 5.3D). Nanoelectrodes with one to 18 nanowires were also fabricated during development of the process (Figure 5.3E and Figure 5.3F). We were able to grow nanowires on platinum-iridium and silver microwires. The spacing between nanowires was chosen so the distance between the furthest nanowires spanned less than a micron, ensuring that all of the nanowires would fit inside a single neuron. We used the residual hydrocarbons in the scanning electron microscope as the precursor for growth, a process known to create nanowires made of metal nanocrystals surrounded by a carbon matrix (Koops et al., 1994).

Next, a 30 nm layer of aluminum oxide was applied using atomic layer deposition (ALD) (Savannah S100, Cambridge NanoTech, Cambridge, MA). Aluminum oxide is an effective insulator often used in glass microelectrodes (Sherman-Gold, 1993). ALD was chosen to ensure high-quality conformal insulation of both the nanowires and the microwire substrate. The electrical properties of a fully insulated nanoelectrode were measured by electrical impedance spectroscopy with a potentiostat (Reference 600, Gamry, Warminster, PA) (Figure 5.4). The nanoelectrode had an impedance of 64 MΩ at 1 kHz, the frequency with the most power in action potentials, and an impedance of 5.7 GΩ at 10 Hz, the frequency important for postsynaptic potentials. The phase angles were measured to be approximately -90° at 1 kHz and -96° at 10 Hz, implying a capacitive electrode.

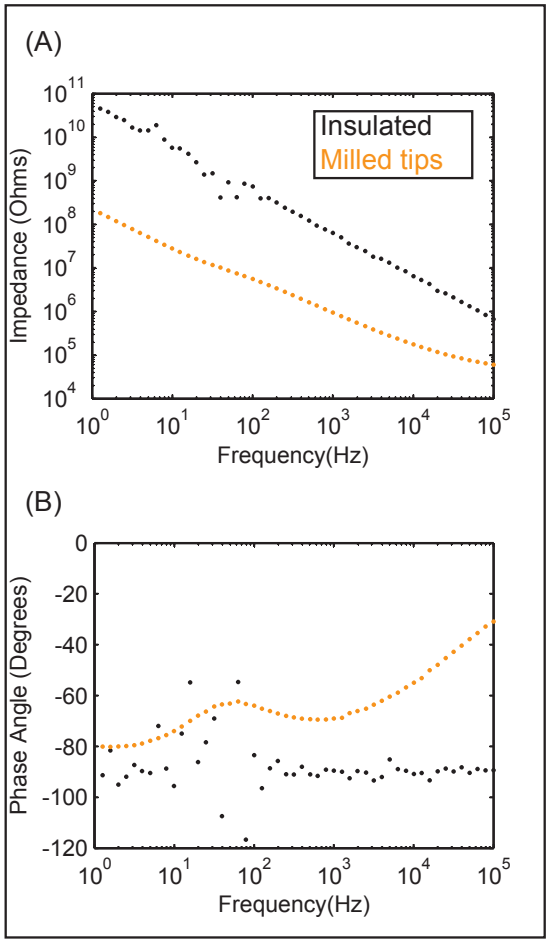

Figure 5.4: *Impedances of the nanoelectrodes. (A) The magnitude of impedance was significantly reduced after the nanowire tips were milled, removing the insulation. (B) The fully insulated nanoelectrode was capacitive, but the milled nanoelectrode had more resistive impedances. From Ferguson et al. (Under review).*

Finally, the tips of the nanowires were milled to remove the insulation using a focused ion beam (FIB) (Quanta 200 3D, FEI, Hillsboro, OR). FIB allowed for selective milling of the tips with complete control on how much of the insulated tip was removed. In most cases, approximately 10–20 nm was removed from the tips of the nanowires. After the insulation was removed from the tips of the nanowires of a nanoelectrode, the impedance magnitudes were measured to be 942 kΩ at 1 KHz and 28 MΩ at 10 Hz, a reduction of two orders of magnitude from the fully insulated nanoelectrode. Also, the phase angles increased to -69° at 1 kHz and -74° at 10 Hz, implying a more resistive electrode.

5.3 Results and discussion

5.3.1 Rat hippocampal slice preparation

To test the nanoelectrodes in a complex natural structure, intracellular action potentials were recorded in spontaneously active CA1 neurons in a rat hippocampal slice preparation (Stigen et al., 2011) (Figure 5.5). The hippocampal slices were 400 microns thick and were visualized using differential interference contrast optics (BX51WI, Olympus, Tokyo, Japan) as the nanoelectrodes approached the target neurons. The nanoelectrodes were connected to a CV-7B headstage of a Multiclamp 700B amplifier (Molecular Devices, Sunnyvale, CA) in current clamp mode to obtain the intracellular recording. A 500 ms buzz was used to help penetrate the neurons. No capacitance compensation was performed. The action

potentials were approximately 15 mV in amplitude and were recorded for several minutes. These action potentials were smaller than those normally obtained with a traditional patch clamp microelectrode because of the large complex impedance of the nanoelectrode or possibly because one or more of the nanowires were located outside the cell, which would cause a shunt pathway. However, the amplitude is consistent with other nanoelectrode recordings of neurons (Schrlau et al., 2009; Hanein et al., 2002). Some of the smaller signals may reflect excitatory postsynaptic potentials rather than action potentials.

5.3.2 Leech ganglion preparation

Intracellular action potentials were also recorded from a touch-sensitive sensory neuron (T cell) of the medicinal leech (*Hirudo verbana*) in an isolated, intact, and desheathed ganglion preparation with nickel solution added to induce bursting (Angstadt and Friesen, 1991) (Figure 5.6A). The T cell was identified by its unique action potential using a sharp microelectrode before the nanoelectrode recording. The nanoelectrode was connected to a standard intracellular recording amplifier (Model 3100, A-M Systems, Sequim, WA). Buzzing assisted the nanoelectrode in penetrating the neuron. Capacitance compensation was not used. The polarity, amplitude, and waveform of the action potentials recorded with the nanoelectrode (Figure 5.6B) were similar to action potentials recorded using a sharp microelectrode. Additionally, extracellular action potentials were recorded as the nanoelectrode approached the cell immediately before the intracellular action potentials

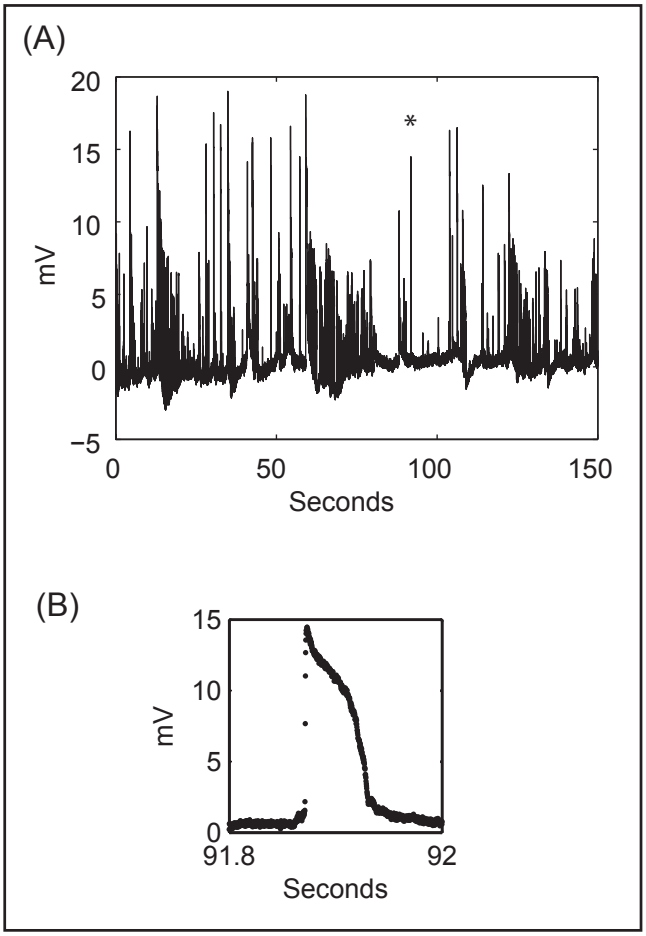

Figure 5.5: *Intracellular recordings in a rat hippocampal slice. (A) 2.5 minutes of action potentials recorded from spontaneously active CA1 neurons. Some of the smaller signals may reflect excitatory postsynaptic potentials. (B) An expanded view of the action potential marked with an asterisk. The waveform is typical of intracellular action potentials recorded without capacitance compensation (Sherman-Gold, 1993). From Ferguson et al. (Under review).*

were recorded. These extracellular action potentials had a primarily negative polarity, opposite to the positive polarity shown by the intracellular action potentials recorded with the nanoelectrode.

After recording, the nanoelectrodes were inspected using a scanning electron microscope (Figure 5.7) following a soak for several hours in a proteolytic enzyme solution (contact lens solution) to remove biological residue. The inspection revealed that all of the nanowires remained intact on every nanoelectrode used. Thus, the nanoelectrodes were robust to insertion into neural tissue.

To re-confirm that recorded action potentials were intracellular, a recording was also obtained from the uniquely identifiable Retzius neurons of the medicinal leech (*Hirudo verbana*). In an isolated but intact ganglion preparation (Puhl and Mesce, 2008), both the nanoelectrode and a traditional glass micropipette were used to record simultaneously the activity of a single Retzius neuron (Figure 5.8A and Figure 5.8B). Both the nanoelectrode and sharp electrode were connected to a standard intracellular recording amplifier (IX2-700, Dagan Instruments, Minneapolis, MN). Buzzing was performed to assist in penetrating the neuron. Capacitance compensation was again not used. The polarity and the timing of the action potentials recorded with the nanoelectrode matched the traditional sharp micropipette recording. However, the amplitudes of these action potentials are smaller than the standard action potentials recorded in Retzius neurons because of damage to the cell from penetration by two electrodes or because of signal shunting (due to the high impedance of the nanoelectrode or some of the nanowires being located outside of the cell during the recording). The record-

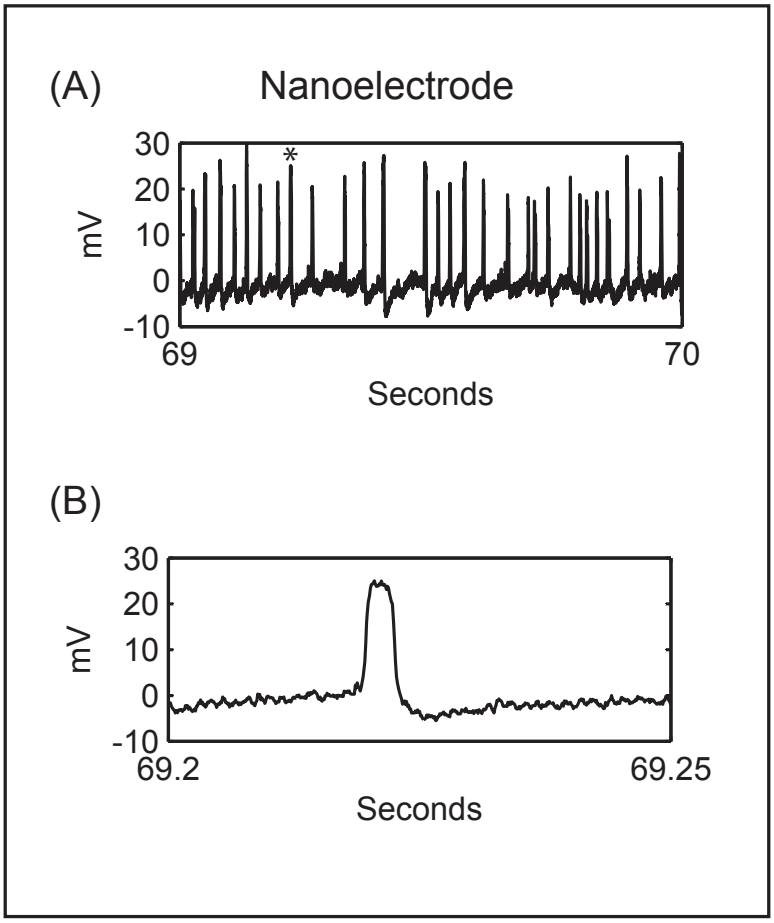

Figure 5.6: *Intracellular action potential recording from a single T cell neuron from an intact ganglion of a medicinal leech (*Hirudo verbana*). From Ferguson et al. (Under review).*

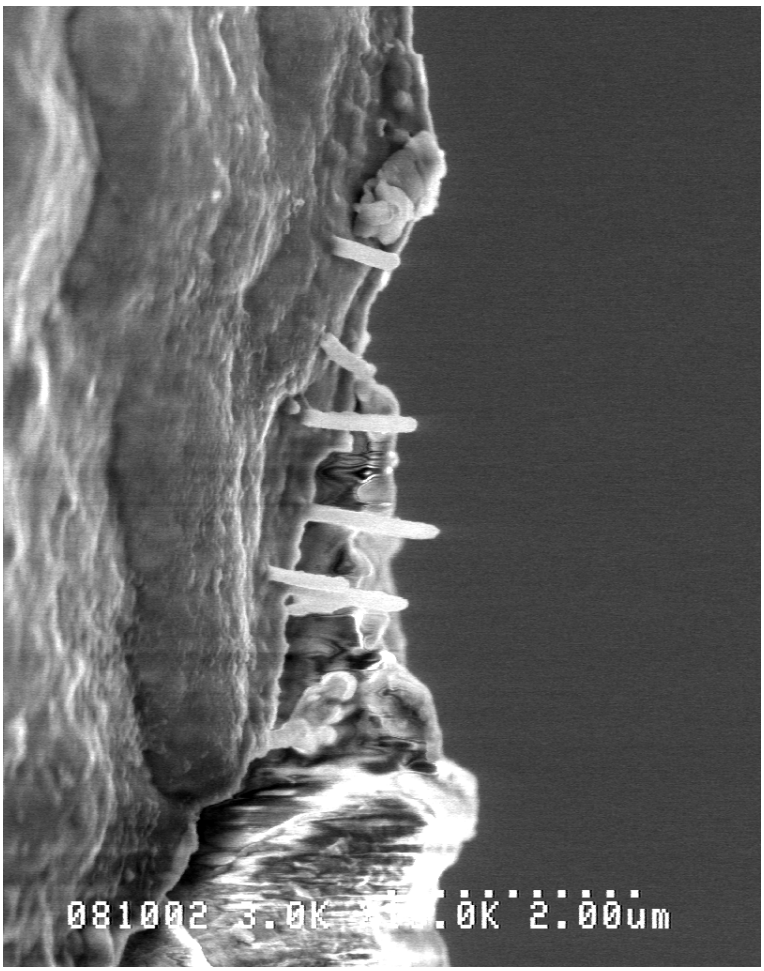

Figure 5.7: *A scanning electron microscope image of a nanoelectrode after being used for recording from the intact ganglion of a medicinal leech (*Hirudo verbana*).*

ings also showed the well-documented smaller amplitude potentials (Figure 5.8C) known to stem from the electrically coupled contralateral homologue (Hagiwara and Morita, 1962). The waveform and polarity of these signals in both traces are indicative of an intracellular-specific recording.

5.4 Conclusions

These results illustrate membrane potential recordings from neurons using a novel nanoelectrode. These nanoelectrodes not only have high aspect ratios and thin and conformal insulation up to the very tip, but they are also highly customizable. The diameter, length, spacing, number, and material composition of the nanowires can be tailored using different EBID scanning parameters or gas precursors (Botman et al., 2009). Also, the thickness of insulation and the area of exposed tips can be controlled with ALD and FIB. Because of this design flexibility, the nanoelectrode can be customized to targeted neurons. A nanoelectrode with more spacing between nanowires can be used for larger cells, and less spacing used for smaller target neurons. Additionally, because the nanoelectrodes are built on supporting microwire structures that have been used for decades to implant chronically and record extracellularly from neural tissues and intact mammalian brains, these nanoelectrodes are potentially well suited for use in neural tissues *in vivo*.

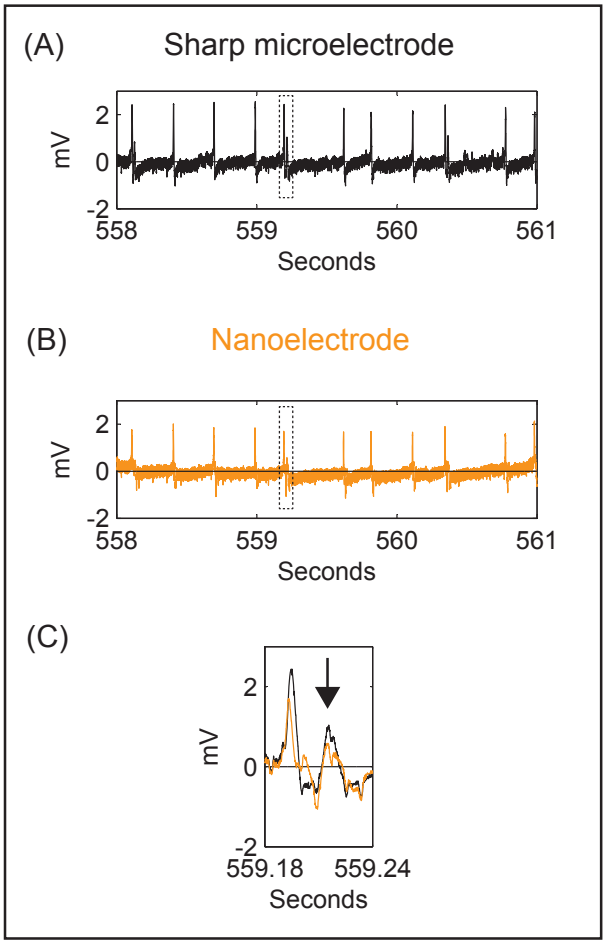

Figure 5.8: *Simultaneous intracellular nanoelectrode and sharp microelectrode recording from a single Retzius neuron from an intact ganglion of a medicinal leech (*Hirudo verbana*). The polarity and timing of the action potentials recorded with the (A) nanoelectrode matched the (B) traditional sharp microelectrode. AC coupling was performed post-recording to remove the baseline drift. (C) The nanoelectrode was also able to record smaller amplitude potentials known to stem from the electrically coupled contralateral homologue (arrow). From Ferguson et al. (Under review).*

Chapter 6

Wireless implantable recording devices

Parts of this chapter have been previously reported in Ferguson and Redish (2011).

6.1 Introduction

Implantable devices for physiological monitoring are widely used by clinicians and researchers to monitor health and to study normal and abnormal body functions. These devices can relay important signals (e.g., ECG, glucose level, blood pressure) from implanted sensors to external equipment to be analyzed or to guide treatment. Implantable devices can also be used to record neural signals in brain-machine interfaces to control prostheses (Velliste et al., 2008) or paralyzed limbs (Moritz et al., 2008).

Communication with implanted devices is usually accomplished with a wired connection or with wireless radiofrequency telemetry. However, wires can break, become infected, or introduce noise in the recording through movement artifacts or by antenna effects. Complications with wires are frequently reported with deep brain stimulation devices (Benabid et al., 2009) and with pacemakers and implantable cardioverter-defibrillators (Hauser et al., 2010).

Wireless radiofrequency (RF) telemetry has been used in several implantable medical devices to avoid the complications of wired implants (Loeb et al., 2006; Orlov et al., 2009). However, wireless RF telemetry requires significant power and suffers from poor transmission through biological tissue. RF telemetry also needs a relatively large antenna, which limits how small the implantable devices can be and prevents implantation in organs such as the brain, heart, and spinal cord without causing significant damage. Other methods of wireless communication have been investigated to communicate with implants, including optical (Murakawa et al., 1999) and ultrasound (Echt et al., 2006). However, these methods also have low efficiency transmission through the body and would be difficult to miniaturize.

Intrabody communication is a recently developed alternative method of wireless communication, which uses the conductive properties of the body to transmit signals. In this chapter, I will explain the major developments and the theory of intrabody communication, describe challenges to putting the technology in practice, and discuss how intrabody communication can be used as the basis for a novel class of wireless implantable medical devices.

6.2 Historical development

The first report of intrabody communication was in 1995 by Zimmerman (1995), where a small signal (approximately 50 pA) was transmitted through the body and detected at a receiving electrode. In this system, a single transmitting and a single receiving electrode were placed near the skin without touching it, capacitively coupled to the body. Another set of electrodes at the transmitter and receiver were also oriented away from the body and were capactively coupled to the environmental ground, serving as the signals return path (Figure 6.1A).

This type of telemetry, called capacitive intrabody communication, has primarily been used for surface-based communication with both the transmitter and receiver electrodes placed on or near the skin. The major limitation of this transmission method is its reliance on capacitive connections to both the body and ground and thus has not been used for communicating with implanted devices. Several applications of capacitive intrabody communication have been developed for transmitting data to consumer electronic devices (Meoli and May-Plumlee, 2002; Hyoung et al., 2006).

The second type of intrabody communication, galvanic, was first reported in 1997 by Handa et al. (1997). A small alternating current flowed from transmitting electrodes on the chest, through the body, and was detected by receiving electrodes on the wrist. The transmitting and receiving electrodes were in direct contact with body, resulting in galvanic coupling (Figure 6.1B). A major advantage of this technology was its very small power requirement, only 8 μW. Also, because

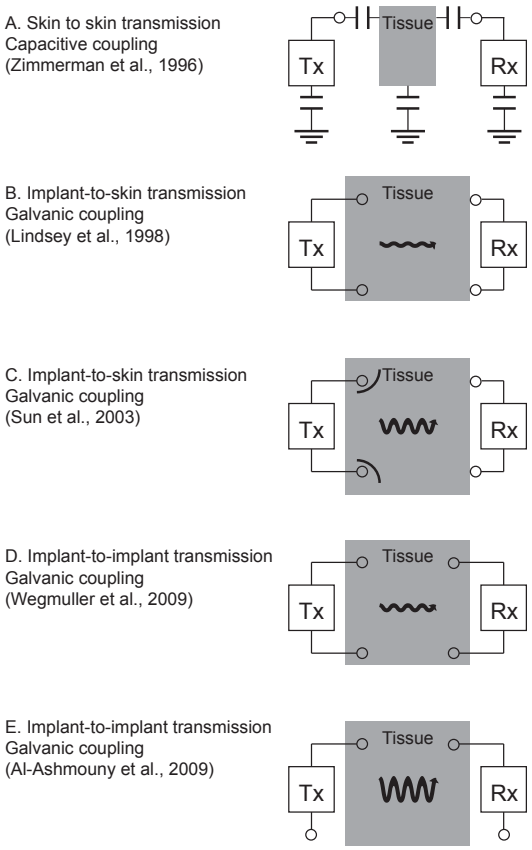

Figure 6.1: *Five types of intrabody communication A. Signal is transmitted from a transmitter (Tx) to a receiver (Rx), both located on the skin, with the body capacitively coupled to the transmitter and receiver electrodes. The transmitter and receiver are also capacitively coupled to the ground, but capacitance between the body and ground reduces the efficiency of signal transmission. B. Signal is transmitted from a transmitter implanted in the tissue to a receiver on the skin. The transmitter and receiver electrodes are galvanically coupled to the tissue. Most of the current passes between the two transmitter electrodes, but sufficient signal transmits across the tissue to be detected by the receiver. C. Using x-antennas to shape the current path, creating a higher impedance path between the transmitter electrodes, stronger signal is detected at the receiver than without x-antennas. D. Signals are detected by an implanted receiver, which reduces signal attenuation and power demands compared to skin-mounted receiver electrodes. E. By using only one transmitter electrode and one receiver electrode galvanically coupled to the tissue, the path between transmitter electrodes has higher impedance than the path to the receiver, resulting in less signal attenuation. High-frequency, charge-balanced, alternating-current signals prevent charge buildup. From Ferguson and Redish (2011).*

no ground connection was required, this type of telemetry could be used with implanted devices.

Galvanic intrabody communication has been studied for a range of medical applications including communicating with implanted and surface-mounted devices. This review will focus on galvanic communication; interested readers can find a recent review of capacitive intrabody communication in (Lučev et al., 2010).

6.3 Surface-to-surface communication

Galvanic coupling can also be used to communicate between devices mounted on the skin. Surface-to-surface communication allows for quick and easy positioning of electrodes, fewer constraints on the size and power demands of the transmitting devices, and avoids surgical implantation. However, because the sensors are on the skin, they may be far from the sources of the signals that are being measured and can result in weak, distorted, or indirect physiological measurements compared to implanted sensors. Nevertheless, these surface-to-surface signals can be combined with signals from implanted devices to create a network of sensors across and inside the body.

6.3.1 Human testing

Because of the convenience and non-invasiveness of surface-to-surface systems, they can easily be tested in humans. Many labs have successfully used galvanic

intrabody communication to transmit data between electrodes attached to the skin (Handa et al., 1997; Song et al., 2010; Wegmueller et al., 2010; Pun et al., 2010).

6.4 Implant-to-surface communication

In implant-to-surface communication, galvanic coupling is used to send signals from an implanted device to electrodes on the skin. This allows for easy placement and repositioning of the skin electrodes to improve the quality of signal reception. However, because the signal has to travel through the skin, which is less conductive than many of the tissues inside the body, more signal attenuation occurs.

6.4.1 Human cadaver testing

Lindsey et al. (1998) tested a method of galvanic communication between an implanted device and surface electrodes to monitor and transmit information about anterior cruciate ligament graft tension after surgery. Two platinum electrodes (each 0.38 mm in diameter, separated by 2.5 mm) were used to inject current into the leg of a human cadaver. EMG electrodes on the surface of the leg were able to detect the transmitted signals. The signals tested were sine waves with frequencies of 2–160 kHz and currents of 1–3 mA, resulting in a minimum signal attenuation of 37 dB. The attenuation increased with smaller currents, with longer distance to the surface electrodes, and with decreased inter-electrode separation of the surface

EMG electrodes. Additionally, the signal attenuation was sensitive to the placement of the surface electrodes in relation to the joint line. Because standard EMG electrodes were used to receive the signal, they could be easily repositioned to improve the quality of signal reception. However, the signal attenuation remained very high (37–50 dB), making signal transmission with high signal-to-noise ratios difficult.

6.4.2 Anesthetized animal testing

A more efficient implant-to-surface communication system was developed by Sun et al. (2003) and tested in saline and an anesthetized pig (Figure 6.1C). The implanted transmitter was integrated in an x-antenna, where the electrodes were integrated in two parabola-like surfaces that altered the current flow. The insulated sections of the x-antenna caused the current to flow in larger paths around the antenna and allowed for more current to be detected at the receiver electrodes. In a saline test, signal delivery using the x-antenna was found to only require 1% of the power of a traditional electrode pair. However, the diameter of the x-antenna was 9 mm, and the transmitter was designed to be implanted on the surface of the brain in between the dura and the cortex, with the signal detected by needle electrodes in the scalp. This system would be too large to be implanted inside the brain without causing significant damage.

6.5 Implant-to-implant communication

In implant-to-implant communication, signals are transmitted from the implanted device to receiver electrodes also implanted inside the body. The implanted receiver can then be connected to equipment outside the body using a short wire or with wireless RF telemetry. In this way, less power is needed to transmit to the implanted receiver electrodes than to electrodes on the skin. However, the implanted receiver electrodes cannot be as easily repositioned as skin-mounted receiver electrodes.

6.5.1 Tissue analogue testing

A system for implant-to-implant communication was developed by Wegmueller et al. (2009) and tested in a muscle-tissue analog (Figure 6.1D). The two electrodes of the transmitter galvanically coupled an alternating-current signal into the body. The signal was then detected by two receiver electrodes. Signals with frequencies of 100–500 kHz were used in order to avoid common neural frequencies, and less than 1 μA of current was used. Two different designs for the transmitting and receiving electrodes were tested: pairs of exposed copper cylinders (10 mm in length and 4 mm in diameter) and exposed copper circles (4 mm in diameter). The electrode sites were spaced 50 mm apart for both the transmitter and receiver. The copper cylinder electrodes could transmit sinusoidal signals with a loss of about 32 dB over 5 cm, and the copper circle electrodes had a loss of 47 dB over 5 cm. However, the electrodes were large and significant signal loss was found with any

misalignment between the transmitter and receiver electrodes. The large signal losses were caused by the four-electrode design; most of the transmitted current returned to the transmitter and did not reach the receiver.

6.5.2 Anesthetized animal testing

A two-electrode system was developed by Al-Ashmouny et al. (2009) and tested in an anesthetized rat (Figure 6.1E). The system used two electrodes in contact with the tissue, one for the transmitter and one for the receiver. Both electrodes were made from 50-μm diameter platinum-iridium wire. The transmitter, an insulated CMOS chip less than $1\,\mathrm{mm}^3$ in volume, was implanted in the rats brain and transmitted alternating-current signals to the receiver electrode, which was also implanted in the brain. More details of the packaging procedure are given in Section 6.6.4. Because the transmitter's circuit ground was insulated from the tissue, the path for current returning to the transmitter had higher impedance than the path through the brain to the receiver. Thus, there was a high-efficiency transfer of the signal to the recording site. Care was taken to use a charge-balanced alternating-current signal in order to avoid charge buildup or tissue damage at the electrode. Using this setup, an encoded neural signal was faithfully transmitted through brain tissue with approximately 20 dB of signal loss. A simultaneous microelectrode recording showed no obvious disruption in activity during signal transmission in the anesthetized rats brain. The two-electrode setup of this system allowed for high efficiency transmission of the signal, but made the system vul-

nerable to extra current sinks in the system. If a low impedance path to ground were present, such as contact between the body and a circuit ground or a grounded water pipe, the signal would be lost.

6.6 Challenges

6.6.1 Power

One of the most difficult challenges for implanted device technologies to overcome is in providing implants with sufficient power to record and transmit signals. However, there has been great progress in understanding how to design miniature low-power circuits for biological applications (Sarpeshkar, 2010). The most common method of powering larger implants such as pacemakers and deep brain stimulation devices is via batteries. However, batteries are difficult to miniaturize and remain the size-limiting component of many implants. Additionally, the lifetime of batteries limits the useful life of potential implants. Battery replacement for implantable devices often requires an additional surgery and can cause many complications. Alternatively, rechargeable batteries allow for longer useful lifetimes but need an additional means of delivering power to recharge, such as RF approaches, which suffer from low efficiency power transfer and require relatively large, aligned antennas.

Other non-RF methods to wirelessly power implanted devices have been proposed but are only in very early stages of development and will require many

advances before they are practical. Witricity, which uses magnetic resonance coupling, allows for highly efficiency energy transfer but requires large coils (Kurs et al., 2007; Zhang et al., 2009). Ultrasound energy can be used to deliver power to implanted devices, but the efficiency of power delivery is very small, around 0.06% (Lee et al., 2007). Energy scavenging (Justin et al., 2004) and optical energy (Murakawa et al., 1999) have also started to be investigated but currently produce too little energy to reliably power implantable devices.

Another approach is to design the implants as passive devices, not requiring any onboard power source. In this approach, the implant acts like an RFID-type device and modulates the signal generated by an external source. The signal then detected outside of the brain includes the information transmitted by the implant. The interrogating signal can be generated by radiative radiofrequency signals like a traditional RFID device (Towe, 2007; Riistama et al., 2009) or using volume conduction (Papale et al., 2010). This approach would allow for the greatest degree of miniaturization since no battery is required. However, early prototypes have used inductors, which are difficult to miniaturize.

6.6.2 Insertion

For a miniature implantable device, alternative approaches to positioning the implant within the body are necessary. The easiest way to insert an implant is by injecting it with a hypodermic needle. This technique is commonly used for implanting RFID tags into the bodies of livestock for identification (Troyk, 1999).

For implantation in the brain, the hard needle protects the implant from the forces encountered when penetrating through dura and brain tissue. However, the volume of brain tissue displaced is larger than if the implant were moved alone. Also, the positive pressure from the syringe may cause damage to tissue. An alternative to a hypodermic needle is to use a vacuum-based tool, similar to the vacuum pickup tools used in placing microelectronic components. In this setup, the implant is held to the tip of a hollow tube by vacuum. Once inserted to the desired depth, the vacuum is released, and the tool is retracted leaving the implant in place.

Another approach to inserting implants is using magnetic guidance, originally developed to guide catheters within the brain (Grady et al., 2000) and for drug delivery of nanoparticles (Neuberger et al., 2005). In magnetic guidance, several large external superconducting magnets control the movement of permanent magnets integrated in the implant. This system allows for control in three dimensions and for easy repositioning of the implant. Non-linear trajectories can even be used to avoid sensitive regions of the brain, which would be impossible in a traditional linear stereotactic approach. However, the implant must be magnetically sensitive, and a complex purpose-built system is required to control the magnetic implant. Another potential concern is unintentional movement of the magnetic implant after implantation due to magnetic forces in the environment or from magnetic resonance imaging.

Dissolvable silk films, which have recently been used to create a mesh for electrodes placed conformably on the brain surface Kim et al. (2010), could also potentially be used in implanting miniature wireless devices. Silk films dissolve

over time, leaving the implant completely unconnected to any wires or fibers. The silk structure attached to the implant can also be used to move or extract the implant during the first few days or weeks before the fibers dissolve. However, the mechanical properties of silk films require further investigation and testing.

6.6.3 Safety

Another important challenge is to minimize the body's response to the implant. Upon recognizing a foreign implant, the body mounts a complex response that occurs on both short and long time scales (Turner et al., 1999; Polikov et al., 2005). This response can adversely affect both the function of the implant and, more importantly, the health of the tissue. Many approaches have been attempted to minimize the tissue response that could also be applied to wireless implantable devices including careful selection of biocompatible materials and coatings (Williams, 2008) and localized drug delivery (Onuki et al., 2008).

It is also important to minimize the effects of intrabody communication on the body, including localized heating caused by power dissipation and unintended stimulation. To avoid the localized heating that can occur with RF telemetry, intrabody communication should use a low frequency carrier wave, ideally below a few MHz. Also, to minimize any unintended stimulation, the frequency of the carrier wave should be above physiologically important frequencies, at least approximately 100 kHz. This range of frequencies between the two bounds also has the advantage of having good quality transmission in biological tissue (Gabriel

et al., 1996a,b,c) and is the frequency range of the tests described in this review. Nevertheless, even at this middle frequency, care must be taken to observe that the specific energy absorption rate and the current density are below the values set in international guidelines (ICNIRP, 1998). Because intrabody communication is a new technology, potential tissue heating and unintended stimulation should be closely monitored in future experiments, even if the transmission is within accepted international standards. In addition, the tissue response to a chronic implant would likely cause an increase in impedance over time at the transmitter as well as an attenuation of the signal at the receiver. Thus, implants should be designed to be robust to changing conditions within the body.

6.6.4 Packaging

A significant challenge in our wireless communication project (Al-Ashmouny et al., 2009) was in packaging the chip. Packaging refers to the process and materials used to prepare the CMOS chip for real-world use. Packaging typically constitutes a significant portion of the size and cost of a chip-based device and can determine the eventual success or failure of the device. In our case, it included 1) connecting the chip to external devices and to a power source, 2) protecting our sensitive chip from the wet biological environment of the brain, and 3) protecting the brain from the electronic circuitry and toxic materials of the chip. Figure 6.2 shows a schematic of the packaging process, which is detailed below.

We received custom-designed Complementary Metal Oxide Semiconductor

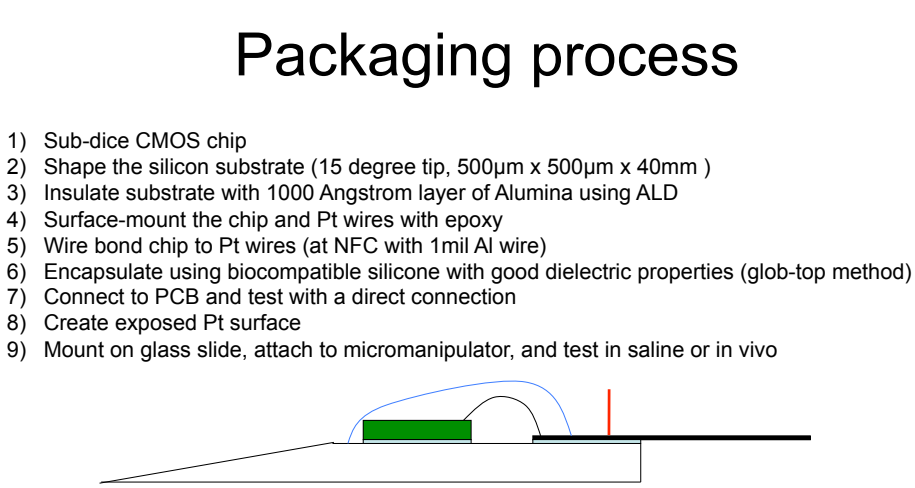

Figure 6.2: *Procedure for packaging a CMOS chip for implantation in a rats brain to test wireless neural communication.*

(CMOS) chips from the MOSIS foundry in large, unpackaged circuit blocks. Our first task in packaging the chips was to cut out the unnecessary parts of the circuit blocks to minimize the device size. To do so, we sub-diced the chip using the diamond wafer saw at the Nanofabrication Center at the University of Minnesota. The chip was placed on top of UV tape (UC-120M-120, 120 microns thick) to help hold it together after cutting. A NBC-ZH 2030-SE diamond blade with 50 micron maximal kerf was used at 4 mm/sec to sub-dice the chip. After a few calibration cuts, the actual kerf was measured and used in conjunction with the optical alignment and micrometer tools on the saw to position the saw for cutting the CMOS chip. After each cut, deionized water and N_2 gas were used to clean the surface. Each cut was visually inspected to ensure the quality of the cut and to confirm that the circuitry was not damaged. After all cuts were completed, the UV

tape was released with a 5 minute exposure to the Oriel flood exposure system at the NFC. The chips were handled using electrostatic-discharge-safe tweezers and grounded wrist bands.

To minimize trauma to brain tissue during insertion and to minimize forces on the chip, the CMOS chip was mounted on a sharp silicon support structure. We chose a chisel-like shape for the tip of the silicon support to allow for easier penetration through the brain (Edell et al., 1992). To create this chisel-shaped support, we diced a 500 micron thick, 100 mm diameter silicon wafer into many smaller pieces with the desired tip angle. We started by making multiple parallel cuts at 500 microns apart using the diamond wafer saw. Then, we made a cut after a fifteen degree rotation of the platform. This resulted in 4–5 cm long spears that had a rectangular cross-section of 500 μm x 500μm and a 15 degree tip angle. We chose the length so the device could reach the hippocampus, deep within the brain. The silicon spears were then insulated with a 1000 Angstrom layer of aluminum oxide on all sides using the atomic layer deposition machine at the NFC.

To connect to the CMOS chip, we used three platinum wires; two were for power and one was for an electrode delivering signal to the neural tissue. The platinum wires had an inner diameter of 50 microns and were insulated with Teflon to an outer diameter of 100 microns (A-M Systems, 771000). The wires were stripped of two centimeters of insulation at one end and were gently tensioned to lay in parallel along the top of a silicon spear. The stripped ends were positioned so that the bare wires ran along the silicon support for three millimeters behind the taper where the insulation began. UV tape (UC-120M-120) in one millimeter

strips was laid atop the wires across the silicon support at roughly one centimeter intervals beginning just behind the taper. Epoxy (GC Electronics, Quik Stik 5 minute) was applied in a thin layer across the tops of the wires avoiding the taped regions and a five millimeter region behind the stripped wires. After curing, we cut the wires 1.5 mm behind the silicon taper and flush at the other end of the silicon support to free the support and wires from the wire tensioning device. The silicon supports were then fixed to a solid surface using double sided tape. A high speed drill turning a 0090 burr (Meisinger, Germany) was used to expose 1 mm of the glued uninsulated platinum wire and create a flat segment on the silicon. A spot of epoxy was then applied to the silicon spear on the 1.5 mm flat segment. The CMOS chip was then set on the glue and adjusted to align the wires with the pads. After curing, the wires were bonded to the chip using 0.001" aluminum wire. Wire bonds that separated prior to encapsulation were reconnected to the Pt wire using conductive epoxy (GC Electronics, Conductive Epoxy Syringe Kit).

To encapsulate the CMOS chip, we chose to use silicone because it is a highly biocompatible material with very good dielectric properties and had previously been shown to be effective in encapsulating neural implants (Donaldson, 1991). We used Dow Corning 3140 silicone to encapsulate the CMOS chip, wire bond wire, and exposed portions of the platinum wire using the glob-top method. We carefully inspected the silicone after application to ensure adequate coverage of all vulnerable surfaces.

For the final steps in packaging, we connected the chip to the external circuitry with direct wire connections. Once the chip's circuit was tested and working prop-

erly, the middle platinum wire was cut, exposing a cross-section of uninsulated platinum wire to the brain. We then epoxied the encapsulated chip to a glass slide using epoxy and soldered the wires to connecting pins. At this point, the chip was fully packaged and ready to be attached to a micromanipulator and lowered into saline or a rats brain for testing (Figure 6.3).

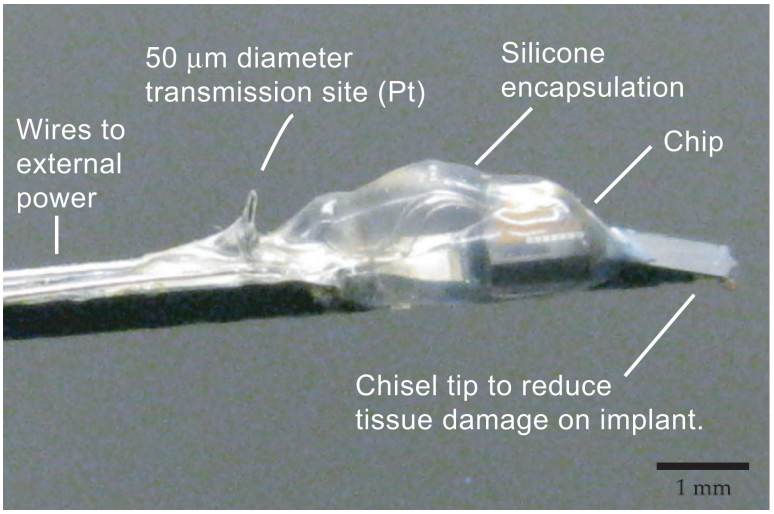

Figure 6.3: *Photograph of the fully packaged CMOS chip ready for implantation. This device was used in Al-Ashmouny et al. (2009).*

The results of the experiment are shown in Figure 6.4. Two battery-powered transmitters, which were the fully packaged CMOS chips as described above, were implanted in an anesthetized rat's brain. One rat was used for this study. These transmitters modulated the prerecorded pseudo-neural signals using binary frequency shift keying at 100/200 kHz for one transmitter and 300/400 kHz for the other transmitter. A battery-powered waystation was also implanted inside the brain and received the signals from the transmitter. The waystation separated the

signals using a band-pass filter and demodulated the signals, resulting in a successful reception of the two signals sent by the transmitters.

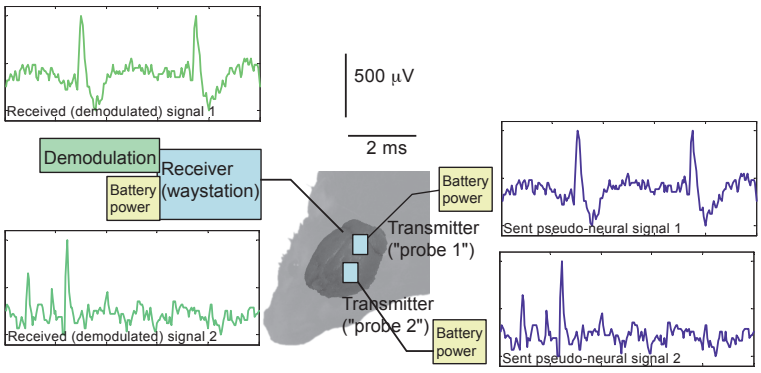

Figure 6.4: *Summary of the experiment performed in Al-Ashmouny et al. (2009). Two prerecorded pseudo-neural signals from two battery-powered transmitters were received by the battery-powered waystation. The received signals were then demodulated and were shown to be equivalent to the transmitted signals.*

6.7 Conclusions

Several approaches to communicating with implanted medical devices using the body as the transmission channel have been proposed and tested. Each of these methods offers some insight in how such a communication system can be realized. Intrabody communication offers several advantages over wires and RF wireless telemetry for communicating with implanted devices. However, intrabody communication is a new technology and several challenges, especially improving power delivery and thoroughly evaluating safety, need to be addressed before it is implanted in humans and used for routine clinical applications like physiological

monitoring.

Because of the body's conductive properties, it can be used as a communication channel to transmit power or information to or from an implant. By eliminating wires, miniature devices can be implanted in multiple structures without restrictions in their positions or be implanted in fragile structures, such as the heart or spinal cord that would be damaged with moving wires. Additionally, the miniature devices could simplify surgical procedures and would help minimize the surgical complications common in implants that use wired connections. Low-power, ultra-miniature implantable devices that use intrabody communication have the potential to enable many exciting applications in the future for both biomedical researchers and clinicians.

Chapter 7

Thoughts on the future of neural recording

This thesis has detailed the current state of neural recording electrodes and our contributions to the field. By working at the nanoscale and with a detailed understanding of the electrical properties of neuron-electrode interfaces, we have shown many significant improvements and novel techniques in ultralow-impedance coatings for extracellular recording electrodes, in nanowires for long-term intracellular recordings, and in wireless communication to extremely small implanted neural recording devices.

However, it is important to remember that neural electrodes serve as tools for researchers and clinicians and are not goals in themselves (although they are great testbeds for investigating scientific questions in many fields including electrochemistry, material science, and micro/nano-fabrication). Rather, the main driv-

ing force for electrode design and development is to enable scientific discoveries and novel/improved medical applications. Therefore, the development of neural electrodes must be made while considering immediate usability and practical applications as well as with an eye to the future.

Many of our results and technological improvements in electrode design have been put into use in our lab and several other labs. This chapter will describe how our contributions are currently being used and speculate how they may develop in the future.

7.1 Nanoscale electrode coatings

Chapter 4 showed our new method for creating a microelectrode coating that reduces the electrode impedance to extremely low levels. The adjustments to the electroplating procedure and the mixing of inhibitory additives are simple to apply and allow for great control over the shape, density, and texture of the coating deposited on the tip of an electrode. We have adopted the ultralow-impedance electroplating method in our lab and have heard many reports of successful adoption of this method from several other labs. However, because of the extra time involvement of this method (plating can take as much as twenty times longer for maximal impedance reduction), we do not always electroplate to the lowest impedance possible. Instead, depending on the target anatomical structure, we usually electroplate to an impedance value much less than the value permitted by traditional electroplating but above the absolute lowest value we can attain.

In the future, I predict that more advanced coating methods will be widely adopted. Not only can ultralow-impedance coatings improve the quality of neural data recorded, but they can also allow for the use of much smaller diameter electrodes than were previously usable for extracellular recordings. This means that it is conceivable to use metal microwire electrodes with diameters on the order of 1 µm or perhaps smaller, rather than the 10–100 µm electrodes that are typically used for stereotrodes and tetrodes. These smaller diameter wires can mean that less tissue is displaced when they are inserted inside the brain. Thus many more microelectrodes can be placed inside brains while minimizing the additional damage. The use of many more (yet smaller) diameter extracellular microelectrodes would be a tremendous advantage for recording large-scale neural ensembles from animals with relatively small brains, such as mice, rats, and songbirds. Also, beyond enabling ultralow-impedance microelectrodes, coatings can enable other functions that would benefit chronic neural recordings. Specifically, coatings can help minimize the chronic tissue response (or at least make it more predicable or controllable). This would greatly benefit a large number of scientists who struggle with chronic tissue responses cutting short a recording experiment before sufficient data is collected. Ideally, in the future, extracellular microelectrode coatings will be fully customizable for each application. In this way, a scientist or clinician could choose the diameter, the impedance, and the mechanical properties of the microelectrode and can additionally control the duration, number of cells recorded per electrode (or recording volume), and types of neural signals recorded for each individual experiment or application.

7.2 Nanoelectrodes

Chapter 5 showed our novel nanoelectrode, which was designed for intracellular recordings. We and many other labs are very excited about the potential of nanoelectrodes, but further development is needed before they are ready for widespread use as a replacement or compliment to traditional intracellular microelectrodes. Many of the design parameters can be further optimized. In particular, I suggest that the next generation of nanoelectrode grows the nanowires from a substrate that is either mechanically polished until it is completely smooth or is tapered using etching. This would help minimize the mechanical disturbance of the nanoelectrode to the neuron being recorded. In any case, it should be recognized that our nanoelectrode served as a very successful prototype. We were able to obtain the first intracellular neural recordings in complex preparations such as leech ganglia and rat hippocampal slices.

In the future, I believe that nanoelectrodes can be used to supplement or replace intracellular recording microelectrodes. Their customizability, small tip size, and ability to be functionalized and grown on nontraditional substrates (e.g., planar surfaces and CMOS pads) are unique advantages. Furthermore, electrode arrays could be developed that combine nanoelectrodes and traditional microwire electrodes to enable simultaneous intracellular and extracellular recordings, especially over long durations. For example, nanoelectrodes can be combined with traditional stereotrodes or tetrodes, which are routinely used for long-duration neural recordings. To do so, nanowires would be grown and partially insulated

on the ends of some microwires, while the other ends would be electroplated traditionally. This hybrid nanoelectrode/microelectrode could allow for simultaneous intracellular and extracellular neural recordings that are much easier to perform than traditional simultaneous recordings. Ultimately, nanoelectrodes can be adapted for *in vivo* recordings and might allow for long-term intracellular recordings of awake, behaving animals. Such technological advances poise to have a significant impact on our current understanding of the physiological underpinnings of nervous system function and on a range of biomedical applications including neuropharmacology, epilepsy, and neural plasticity research.

7.3 Miniature implantable devices

The wireless communication system described in Chapter 6 is also in early stages of development with many exciting future potential uses. We are still building early prototypes of the device and are investigating some of the challenges described in Chapter 6, such as power, insertion methods, and safety. In the near future, the likeliest users of intrabody communication will be biomedical research labs that will investigate the capabilities of the technology and develop applications for small animal studies, where miniature implantable sensors are vital for many research questions.

Further in the future, a novel form of physiological monitoring can be envisioned, where multiple ultra-miniature implants are located in various locations in the body. These implants can be interrogated using an RFID-type telemetry sys-

tem. By making each implant sensitive only to a specific frequency range, the implants can be made individually addressable and be used in a body-wide network. Such a system of implantable devices would allow for flexible positioning options without the restrictions and problems of wires and could enable access to tissues sensitive to movement such as the heart and spinal cord. One potential vision for this system is a network of injectable, miniature wireless neural implants (Figure 7.1). By being wireless and miniature, they would allow researchers to have complete freedom in selecting the locations of neural recording sites. Since most neurological diseases affect multiple brain regions, being able to monitor neural activity and observe intra-region communication is likely to be important to our understanding of dysfunction. For example, multiple injectable neural recording implants in and around the focus of seizure activity would be beneficial in surgical planning or monitoring for epilepsy patients. As a final speculative vision of the future of neural recording technology, recording from neurons might be as simple as injecting a solution filled with neural recording devices into the bloodstream of the patient or subject. The devices can then navigate to and recognize their target. Finally, they can faithfully record and wirelessly transmit neural recording data without damaging neurons or affecting their natural function. This may sound like science fiction today, but is quite possible in the future, given the continual miniaturization and improvement of neural recording technology enabled by a deeper understanding of the issues involved. This thesis, as stated in the introduction, is a step in that direction, by attempting to stand on the shoulders of giants and to look at the nanoscale.

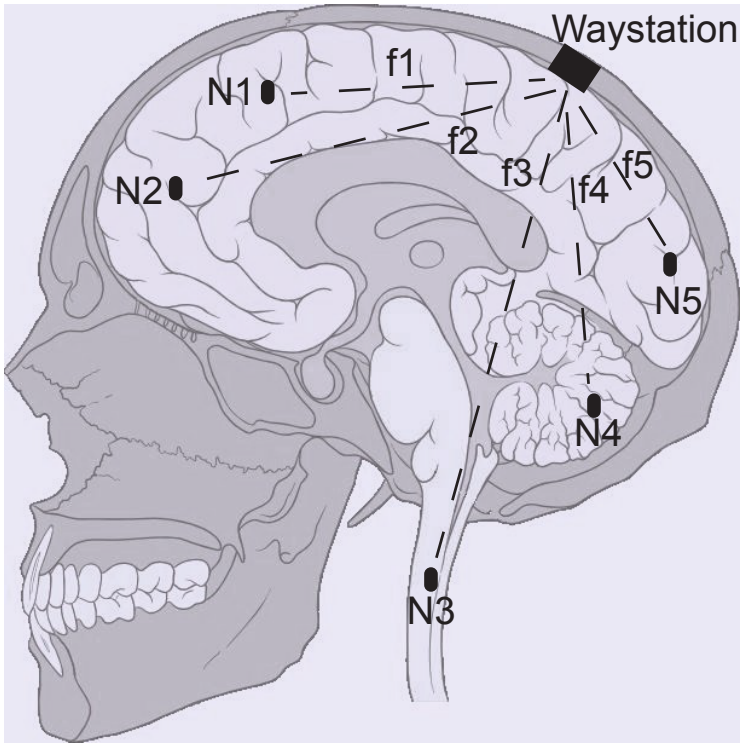

Figure 7.1: *A possible future vision for wireless, miniature implantable devices for neurological monitoring applications, different from any currently available technologies. Several implants (N1-N5) are injected in the brain and spinal cord. The implants are tuned to specific frequencies (f1-f5) and thus are individually addressable. The receiver, the waystation, allows for communication between multiple implants and external devices, and, because it is implanted, it improves the transmission efficiency. This technology could enable the development of novel tools for neuroscience research and clinical care. From Ferguson and Redish (2011). Background image by Patrick J. Lynch. License: GFDL. Source: Wikimedia Commons.*

Bibliography

Al-Ashmouny, K. M., Boldt, C., Ferguson, J. E., Erdman, A. G., Redish, A. D., and Yoon, E. (2009). IBCOM (intra-brain communication) microsystem: Wireless transmission of neural signals within the brain. In *Proc. Annual Int. Conf. of the IEEE Engineering in Medicine and Biology Society*, pages 2054–2057.

Angstadt, J. D. and Friesen, W. O. (1991). Synchronized oscillatory activity in leech neurons induced by calcium channel blockers. *J. Neurophysiol.*, 66(6):1858–73.

Benabid, A. L., Chabardes, S., Mitrofanis, J., and Pollak, P. (2009). Deep brain stimulation of the subthalamic nucleus for the treatment of Parkinson's disease. *Lancet Neurol*, 8(1):67–81.

Botman, A., Mulders, J. J. L., and Hagen, C. W. (2009). Creating pure nanostructures from electron-beam-induced deposition using purification techniques: a technology perspective. *Nanotechnology*, 20(37):372001.

Brown, K. T. and Flaming, D. G. (1986). *Advanced micropipette techniques for cell physiology*. Wiley, London.

Cogan, S. F. (2008). Neural stimulation and recording electrodes. *Annu Rev Biomed Eng*, 10:275–309.

Cui, X. and Martin, D. C. (2003). Fuzzy gold electrodes for lowering impedance and improving adhesion with electrodeposited conducting polymer films. *Sensors & Actuators: A. Physical*, 103(3):384–394.

de Asis, E. D., Leung, J., Wood, S., and Nguyen, C. V. (2009). High spatial resolution single multiwalled carbon nanotube electrode for stimulation, recording, and whole cell voltage clamping of electrically active cells. *Appl. Phys. Lett.*, 95(15):153701.

Donaldson, P. E. (1991). Aspects of silicone rubber as an encapsulant for neurological prostheses. Part 1. Osmosis. *Med Biol Eng Comput.*, 29(1):34–39.

Echt, D. S., Cowan, M. W., Riley, R. E., and Brisken, A. F. (2006). Feasibility and safety of a novel technology for pacing without leads. *Heart Rhythm*, 3(10):1202–1206.

Edell, D. J., Toi, V. V., McNeil, V. M., and Clark, L. D. (1992). Factors influencing the biocompatibility of insertable silicon microshafts in cerebral cortex. *IEEE transactions on bio-medical engineering*, 39(6):635–43.

Ettisch, G. and Péterfi, T. (1925). Zur Methodik der Elektrometrie der Zelle. *PFLÜGERS ARCHIV EUROPEAN JOURNAL OF PHYSIOLOGY*, 208(1):454–466.

Fatt, P. (1957). Electric potentials occurring around a neurone during its antidromic activation. *Journal of Neurophysiology*, 20(1):27.

Feltham, A. M. and Spiro, M. (1971). Platinized platinum electrodes. *Chem Rev*, 71(2):177–193.

Ferguson, J., Boldt, C., Puhl, J., Stigen, T., Jackson, J., Crisp, K., Mesce, K., Netoff, T., and Redish, A. Neuronal action potentials recorded intracellularly with nanoelectrodes.

Ferguson, J. E., Boldt, C., and Redish, A. D. (2009). Creating low-impedance tetrodes by electroplating with additives. *Sensors and actuators. A: Physical*, 156(2):388–393.

Ferguson, J. E. and Redish, A. D. (2011). Wireless communication with implanted medical devices using the conductive properties of the body. *Expert Review of Medical Devices*, 8(4):427–433.

Ferris, C. F. (1974). *Introduction to Bioelectrodes*. Plenum Press, New York.

Freygang, W. and Frank, K. (1959). Extracellular potentials from single spinal motoneurons. *The Journal of General Physiology*, 42(4):749.

Gabriel, C., Gabriel, S., and Corthout, E. (1996a). The dielectric properties of biological tissues: I. Literature survey. *Physics in medicine and biology*, 41(11):2231–49.

Gabriel, S., Lau, R. W., and Gabriel, C. (1996b). The dielectric properties of biological tissues: II. Measurements in the frequency range 10 Hz to 20 GHz. *Physics in medicine and biology*, 41(11):2251–69.

Gabriel, S., Lau, R. W., and Gabriel, C. (1996c). The dielectric properties of biological tissues: III. Parametric models for the dielectric spectrum of tissues. *Physics in medicine and biology*, 41(11):2271–93.

Geddes, L. A. (1972). *Electrodes and the Measurement of Bioelectric Events*. John Wiley & Sons.

Gelfan, S. (1926). A non-polarizable micro-electrode. *Proceedings of the Society for Experimental Biology and Medicine*, 23:308–309.

Gold, C., Henze, D. a., and Koch, C. (2007). Using extracellular action potential recordings to constrain compartmental models. *Journal of computational neuroscience*, 23(1):39–58.

Gold, C., Henze, D. a., Koch, C., and Buzsáki, G. (2006). On the origin of the extracellular action potential waveform: A modeling study. *Journal of neurophysiology*, 95(5):3113–28.

Grady, M. S., Howard, M. A., Dacey, R. G., Blume, W., Lawson, M., Werp, P., and Ritter, R. C. (2000). Experimental study of the magnetic stereotaxis system for catheter manipulation within the brain. *J Neurosurg*, 93(2):282–288.

Gray, C. M., Maldonado, P. E., Wilson, M., and McNaughton, B. (1995). Tetrodes markedly improve the reliability and yield of multiple single-unit isolation from multi-unit recordings in cat striate cortex. *J Neurosci Methods*, 63(1-2):43–54.

Hagiwara, S. and Morita, H. (1962). Electronic transmission between two nerve cells in leech ganglion. *J. Neurophysiol.*, 25:721–731.

Hamill, O. P., Marty, A., Neher, E., Sakmann, B., and Sigworth, F. J. (1981). Improved patch-clamp techniques for high-resolution current recording from cells and cell-free membrane patches. *Pflügers Arch.*, 391(2):85–100.

Handa, T., Shoji, S., Ike, S., Takeda, S., and Sekiguchi, T. (1997). A very low-power consumption wireless ECG monitoring system using body as a signal transmission medium. *Int Solid St Sensor Actuator Conf*, pages 1003–1006.

Hanein, Y., Böhringer, K., Wyeth, R., and Willows, A. (2002). *Towards MEMS probes for intracellular recording.*, volume 10, pages 47–75.

Hauser, R. G., Katsiyiannis, W. T., Gornick, C. C., Almquist, A. K., and Kallinen, L. M. (2010). Deaths and cardiovascular injuries due to device-assisted implantable cardioverter-defibrillator and pacemaker lead extraction. *Europace*, 12(3):395–401.

Henze, D. A., Borhegyi, Z., Csicsvari, J., Mamiya, A., Harris, K. D., and Buzsáki, G. (2000). Intracellular features predicted by extracellular recordings in the hippocampus in vivo. *J Neurophysiol*, 84(1):390–400.

Hodgkin, A. and Huxley, A. (1952). A quantitative description of membrane current and its application to conduction and excitation in nerve. *The Journal of physiology*, 117(4):500.

Horn, R. and Marty, a. (1988). Muscarinic activation of ionic currents measured by a new whole-cell recording method. *The Journal of general physiology*, 92(2):145–59.

Hyoung, C. H., Sung, J. B., Hwang, J. H., Kim, J. K., Park, D. G., and Kang, S. W. (2006). A novel system for intrabody communication: touch-and-play. In *IEEE Int Symp Circs*.

ICNIRP (1998). Guidelines for limiting exposure to time-varying electric, magnetic, and electromagnetic fields (up to 300 GHz). *Health Physics*, 74(4):494–522.

Janders, M., Egert, U., Stelzle, M., and Nisch, W. (1996). Novel thin film titanium nitride micro-electrodes with excellent charge transfer capability for cell stimulation and sensing applications. In *Proc. 18th Annual International Conference of the IEEE Bridging Disciplines for Biomedicine Engineering in Medicine and Biology Society*, volume 1, pages 245—-247 vol.1.

Justin, G. A., Zhang, Y., Sun, M., and Sclabassi, R. (2004). Biofuel cells: a possible power source for implantable electronic devices. In *Proc. 26th Annual Int. Conf. of the IEEE Engineering in Medicine and Biology Society*, volume 2, pages 4096–4099.

Keefer, E. W., Botterman, B. R., Romero, M. I., Rossi, A. F., and Gross, G. W. (2008). Carbon nanotube coating improves neuronal recordings. *Nat Nanotechnol*, 3(7):434–439.

Kim, D.-H., Viventi, J., Amsden, J. J., Xiao, J., Vigeland, L., Kim, Y.-S., Blanco, J. A., Panilaitis, B., Frechette, E. S., Contreras, D., Kaplan, D. L., Omenetto, F. G., Huang, Y., Hwang, K.-C., Zakin, M. R., Litt, B., and Rogers, J. A. (2010). Dissolvable films of silk fibroin for ultrathin conformal bio-integrated electronics. *Nat Mater*, 9(6):511–517.

Kim, W., Ng, J. K., Kunitake, M. E., Conklin, B. R., and Yang, P. (2007). Interfacing silicon nanowires with mammalian cells. *J. Am. Chem. Soc.*, 129(23):7228–7229.

Koops, H. W. P., Kretz, J., Rudolph, M., Weber, M., Dahm, G., and Lee, K. L. (1994). Characterization and application of materials grown by electron-beam-induced deposition. *Jpn. J. Appl. Phs.*, 33:7099–7107.

Kurs, A., Karalis, A., Moffatt, R., Joannopoulos, J. D., Fisher, P., and Soljacic, M. (2007). Wireless power transfer via strongly coupled magnetic resonances. *Science*, 317(5834):83–86.

Lee, K. L., Lau, C.-P., Tse, H.-F., Echt, D. S., Heaven, D., Smith, W., and Hood, M. (2007). First human demonstration of cardiac stimulation with transcutaneous ultrasound energy delivery: implications for wireless pacing with implantable devices. *J Am Coll Cardiol*, 50(9):877–883.

Lin, K., Weil, R., and Desai, K. (1986). Effects of Current Density, Pulse Plating, and Additives on the Initial Stage of Gold Deposition. *Journal of The Electrochemical Society*, 133:690.

Lindsey, D. P., McKee, E. L., Hull, M. L., and Howell, S. M. (1998). A new technique for transmission of signals from implantable transducers. *IEEE T Bio-Med Eng*, 45(5):614–619.

Loeb, G. E., Peck, R. A., and Martyniuk, J. (1995). Toward the ultimate metal microelectrode. *J Neurosci Methods*, 63(1-2):175–183.

Loeb, G. E., Richmond, F. J. R., and Baker, L. L. (2006). The BION devices: injectable interfaces with peripheral nerves and muscles. *Neurosurg Focus*, 20(5):1–9.

Ludwig, K. A., Uram, J. D., Yang, J., Martin, D. C., and Kipke, D. R. (2006). Chronic neural recordings using silicon microelectrode arrays electrochemically deposited with a poly(3,4-ethylenedioxythiophene) (PEDOT) film. *J Neural Eng*, 3(1):59–70.

Lučev, Z., Krois, I., and Cifrek, M. (2010). Intrabody Communication in

Biotelemetry. *Wearable and Autonomous Biomedical Devices and Systems for Smart Environment.*, pages 351–368.

McConnell, G. C., Rees, H. D., Levey, A. I., Gutekunst, C.-A., Gross, R. E., and Bellamkonda, R. V. (2009). Implanted neural electrodes cause chronic, local inflammation that is correlated with local neurodegeneration. *Journal of neural engineering*, 6(5):056003.

McNaughton, B. L., O'Keefe, J., and Barnes, C. a. (1983). The stereotrode: a new technique for simultaneous isolation of several single units in the central nervous system from multiple unit records. *Journal of neuroscience methods*, 8(4):391–7.

Mechler, F. and Victor, J. (2011). Dipole characterization of single neurons from their extracellular action potentials. *Journal of Computational Neuroscience*, pages 1–28.

Mechler, F., Victor, J., Ohiorhenuan, I., Schmid, A., and Hu, Q. (2011). Three-dimensional Localization of Neurons in Cortical Tetrode Recordings. *Journal of Neurophysiology*.

Meoli, D. and May-Plumlee, T. (2002). Interactive electronic textile development: A review of technologies. *J Text Apparel Technol Manag*, 2(2):1–12.

Merrill, E. G. and Ainsworth, A. (1972). Glass-coated platinum-plated tungsten microelectrodes. *Med Biol Eng*, 10(5):662–672.

Milstein, J. and Koch, C. (2008). Dynamic moment analysis of the extracellular electric field of a biologically realistic spiking neuron. *Neural computation*, 20(8):2070–2084.

Moritz, C. T., Perlmutter, S. I., and Fetz, E. E. (2008). Direct control of paralysed muscles by cortical neurons. *Nature*, 456(7222):639–642.

Murakawa, K., Kobayashi, M., Nakamura, O., and Kawata, S. (1999). A wireless near-infrared energy system for medical implants. *IEEE Eng Med Biol*, 18(6):70–72.

Neher, E. and Sakmann, B. (1976). Single-channel currents recorded from membrane of denervated frog muscle fibres. *Nature*, 260:799–802.

Nelson, M. J., Pouget, P., Nilsen, E. A., Patten, C. D., and Schall, J. D. (2008). Review of signal distortion through metal microelectrode recording circuits and filters. *J Neurosci Methods*, 169:141–157.

Neuberger, T., Schöpf, B., Hofmann, H., Hofmann, M., and Von Rechenberg, B. (2005). Superparamagnetic nanoparticles for biomedical applications: Possibilities and limitations of a new drug delivery system. *J Magn Magn Mater*, 293:483–496.

O'Keefe, J. and Dostrovsky, J. (1971). The hippocampus as a spatial map. Preliminary evidence from unit activity in the freely-moving rat. *Brain research*, 34:171–175.

O'Keefe, J. and Recce, M. L. (1993). Phase relationship between hippocampal place units and the EEG theta rhythm. *Hippocampus*, 3(3):317–330.

Onuki, Y., Bhardwaj, U., Papadimitrakopoulos, F., and Burgess, D. J. (2008). A review of the biocompatibility of implantable devices: current challenges to overcome foreign body response. *J Diabetes Sci Technol*, 2(6):1003–15.

Orlov, M. V., Szombathy, T., Chaudhry, G. M., and Haffajee, C. I. (2009). Remote surveillance of implantable cardiac devices. *PACE*, 32(7):928–39.

Papale, A., Ferguson, J. E., Boldt, C., and Redish, A. D. (2010). Steps toward decoupling ensemble recording sites from the headstage. In *Society for Neuroscience Annual Conference*.

Polikov, V. S., Tresco, P. A., and Reichert, W. M. (2005). Response of brain tissue to chronically implanted neural electrodes. *J Neurosci Methods*, 148(1):1–18.

Puhl, J. G. and Mesce, K. A. (2008). Dopamine activates the motor pattern for crawling in the medicinal leech. *J. Neurosci.*, 28(16):4192–200.

Pun, S. H., Gao, Y. M., Mou, P. a., Mak, P. U., Vai, M. I., and Du, M. (2010). Multilayer limb quasi-static electromagnetic modeling with experiments for Galvanic coupling type IBC. *Conference proceedings : ... Annual International Conference of the IEEE Engineering in Medicine and Biology Society. IEEE Engineering in Medicine and Biology Society. Conference*, 1:378–81.

Purves, R. D. (1981). *Microelectrode methods for intracellular recording and ionophoresis*. Academic Press, London.

Riistama, J., Aittokallio, E., Verho, J., and Lekkala, J. (2009). Totally passive wireless biopotential measurement sensor by utilizing inductively coupled resonance circuits. *Sensor Actuat A-Phys*, 157:313–321.

Robinson, D. A. (1968). The electrical properties of metal microelectrodes. *Proc IEEE*, 56(6):1065–1071.

Sarpeshkar, R. (2010). *Ultra low power bioelectronics: fundamentals, biomedical applications, and bio-inspired systems*. Cambridge University Press, Cambridge, UK.

Schönenberger, C., van der Zande, B., Fokkink, L., Henny, M., Shmid, C., Krüger, M., Bachtold, A., and Huber (1997). Template Synthesis of Nanowires in Porous Polycarbonate Membranes: Electrochemistry and Morphology. *The Journal of Physical Chemistry B*, 101(28):5497–5505.

Schrlau, M. G., Dun, N. J., and Bau, H. H. (2009). Cell electrophysiology with carbon nanopipettes. *ACS Nano*, 3(3):563–568.

Sherman-Gold, R. (1993). *The Axon Guide*. Axon Instruments, Inc.

Song, Y., Hao, Q., Zhang, K., Wang, M., Chu, Y., and Kang, B. (2010). The Simulation Method of the Galvanic Coupling Intrabody Communication With

Different Signal Transmission Paths. *Ieee Transactions On Instrumentation And Measurement*, pages 1–10.

Stice, P. and Muthuswamy, J. (2009). Assessment of gliosis around moveable implants in the brain. *Journal of neural engineering*, 6(4):046004.

Stigen, T., Danzl, P., Moehlis, J., and Netoff, T. (2011). Controlling spike timing and synchrony in oscillatory neurons. *J. Neurophysiol.*

Stock, B. (1979). Antiqui and Moderni as "Giants" and "Dwarfs": A Reflection of Popular Culture? *Modern Philology*, 76(4):370–374.

Stoychev, D. and Tsvetanov, C. (1996). Behaviour of poly (ethylene glycol) during electrodeposition of bright copper coatings in sulfuric acid electrolytes. *J Appl Electrochem*, 26(7):741–749.

Strumwasser, F. (1958). Long-term recording from single neurons in brain of unrestrained mammals. *Science*, 127(3296):469–470.

Sun, M., Mickle, M., Liang, W., Liu, Q., and Sclabassi, R. J. (2003). Data communication between brain implants and computer. *IEEE T Neur Sys Reh*, 11(2):189–192.

Sun, P., Laforge, F. O., Abeyweera, T. P., Rotenberg, S. A., Carpino, J., and Mirkin, M. V. (2008). Nanoelectrochemistry of mammalian cells. *Proc. Nat. Acad. Sci. U.S.A.*, 105(2):443–8.

Suner, S., Fellows, M. R., Vargas-Irwin, C., Nakata, G. K., and Donoghue, J. P. (2005). Reliability of signals from a chronically implanted, silicon-based electrode array in non-human primate primary motor cortex. *IEEE Trans Neural Syst Rehabil Eng*, 13(4):524–541.

Terzuolo, C. and Araki, T. (1961). An analysis of intra-versus extracellular potential changes associated with activity of single spinal motoneurons. *Annals of the New York Academy of Sciences*, 94(2):547–558.

Tian, B., Cohen-Karni, T., Qing, Q., Duan, X., Xie, P., and Lieber, C. M. (2010). Three-dimensional, flexible nanoscale field-effect transistors as localized bioprobes. *Science*, 329(5993):830–834.

Towe, B. C. (2007). Passive Backscatter Biotelemetry for Neural Interfacing. In *Proc. 3rd Int. IEEE/EMBS Conf. Neural Engineering*, pages 144–147.

Troyk, P. R. (1999). Injectable electronic identification, monitoring, and stimulation systems. *Annu Rev Biomed Eng*, 1:177–209.

Turner, J. N., Shain, W., Szarowski, D. H., Andersen, M., Martins, S., Isaacson, M., and Craighead, H. (1999). Cerebral astrocyte response to micromachined silicon implants. *Exp Neurol*, 156(1):33–49.

Velliste, M., Perel, S., Spalding, M. C., Whitford, A. S., and Schwartz, A. B. (2008). Cortical control of a prosthetic arm for self-feeding. *Nature*, 453(7198):1098–1101.

Wegmueller, M. S., Huclova, S., Froehlich, J., Oberle, M., Felber, N., Kuster, N., and Fichtner, W. (2009). Galvanic Coupling Enabling Wireless Implant Communications. *IEEE T Instrum Meas*, 58(8):2618–2625.

Wegmueller, M. S., Oberle, M., Felber, N., Kuster, N., and Fichtner, W. (2010). Signal Transmission by Galvanic Coupling Through the Human Body. *IEEE T Instrum Meas*, 59(4):963–969.

Weil, R. (1989). The Structures of Electrodeposits and the Properties that Depend on Them. *Annual Reviews in Materials Science*, 19(1):165–182.

Williams, D. F. (2008). On the mechanisms of biocompatibility. *Biomaterials*, 29(20):2941–53.

Williams, J. C., Hippensteel, J. A., Dilgen, J., Shain, W., and Kipke, D. R. (2007). Complex impedance spectroscopy for monitoring tissue responses to inserted neural implants. *J Neural Eng*, 4(4):410–423.

Wilson, M. A. and McNaughton, B. L. (1993). Dynamics of the hippocampal ensemble code for space. *Science*, 261(5124):1055–1058.

Winand, R. (1994). Electrodeposition of metals and alloys-new results and perspectives. *Electrochim Acta*, 39:1091.

Wise, K., Angell, J., and Starr, A. (1970). An integrated-circuit approach to extracellular microelectrodes. *Biomedical Engineering, IEEE Transactions on*, (3):238–247.

Wise, K. D. (2007). Integrated sensors, MEMS, and microsystems: Reflections on a fantastic voyage. *Sensors & Actuators: A. Physical*, 136(1):39–50.

Ypey, D. L. and DeFelice, L. J. (2011). *The patch-clamp technique explained and exercise with the use of simple electrical equivalent circuits*.

Zhang, F., Liu, X., Hackworth, S. A., Sclabassi, R. J., and Sun, M. (2009). In vitro and in vivo studies on wireless powering of medical sensors and implantable devices. In *Proc. IEEE/NIH Life Science Systems and Applications Workshop*, pages 84–87.

Zimmerman, T. G. (1995). *Personal Area Networks (PAN): Near-Field Intra-Body Communication*. PhD thesis, Massachusetts Institute of Technology.